Chapter XX
Magnetism of Low-dimensional Metallic Structures

Q1

●A. Enders[1], P. Gambardella[2,3] and K. Kern[1,2]

[1] *Max Planck Institut für Festkörperforschung, Stuttgart, Germany*
[2] *Ecole Polytechnique Fédérale de Lausanne (EPFL), Lausanne, Switzerland*
[3] *Catalan Institute of Research and Advanced Studies (ICREA), Barcelona, Spain*

1 INTRODUCTION

Many elements in the periodic table show a magnetic moment as free atoms. However, only iron, cobalt, nickel, and a few rare-earths and their alloys exhibit ferromagnetic properties in bulk compounds. The evolution of the atomic magnetic moments, their mutual coupling (which ultimately produces macroscopic magnetism), and the appearance of magnetic anisotropy in molecules, nanosized aggregates, and solids are the subjects of intense investigation. Besides being of fundamental interest, such questions bear on the design of novel magnetic devices with one or more dimensions reduced to the length scale of interatomic cooperative magnetic behavior. Understandably, we have good theoretical models and plenty of experimental data that tell us how magnetism works in free atoms and crystalline solids. However, as we explore the realm in between these two limits, we face a remarkable paucity of experimental information. The relevant length scale of the exchange interaction in most magnetic materials is only a few atomic spacings. This is the reason why the exploration of magnetic nanostructures has traditionally lagged behind the semiconductor field. Whereas in semiconductors the dimensions of the system influence the charge carriers' behavior already for typical lengths of tens of nanometers, magnetic materials must be engineered down to the Angstrom scale. It is only in the last two decades that advances in growth and characterization methods have allowed us to investigate and produce artificial structures with magnetic properties controlled with nanometer precision. Such progress has given rise to a wealth of technological applications, of which the most relevant are of giant magnetoresistance that is, currently used in sensors and in the read-heads of computer hard disks, spin-based electronics, of great promise for integrated memory and electronic devices and the conception of new magnetic media.

Here, we are concerned with fundamental issues that govern the magnetic behavior of nanostructured materials as well as that of magnetic alloys down to the ultimate atomic scale. First, we describe the fabrication and the magnetic properties of zero-dimensional (0D), one-dimensional (1D), and two-dimensional (2D) nanostructures of Co and Fe, outlining the governing principles for self-organized growth of metallic nanostructures on crystalline substrates. By exploiting the hierarchy of diffusion processes on flat and stepped metal surfaces, we are able to construct low-dimensional magnetic systems almost atom-by-atom, which gives us an unprecedented view on the evolution of magnetization, magnetic anisotropy,

Handbook of Magnetism and Advanced Magnetic Materials, Edited by Helmut Kronmüller and Stuart Parkin. Volume 1: *Fundamentals and Theory*. ISBN: 978-0-470-02217-7.

and magnetic order from atoms to solids. Starting from individual impurities, we let ensembles of dimers, trimers, and larger clusters self-assemble by controlling their coverage and substrate temperature. Surfaces with regular arrays of monatomic steps are used to induce the formation of 1D atomic chains. With increasing coverage the chains evolve into stripes in a row-by-row fashion, and finally into 2D atomically thin layers. The investigation of such structures has revealed exciting and unexpected properties. As one important result we demonstrate how the superparamagnetic limit – encountered in samples too small to provide sufficient long-term stability of ferromagnetic order and a well-known limit to the increase of the bit density in magnetic memories – can be elegantly circumvented in nanostructures. The key is in the very large magnetic anisotropy of some of the nanostructures, which results from their reduced atomic coordination on one hand, and the electronic hybridization with substrate atoms on the other hand. The discussed examples demonstrate how nanoscale structures can provide practical solutions to elude classical difficulties in the use of magnetic materials as well as fundamental input to our understanding of magnetic phenomena.

2 SELF-ORGANIZED GROWTH OF METALLIC NANOSTRUCTURES

Common to all bottom-up strategies for the fabrication of metallic nanostructures at surfaces is that they are essentially based on growth phenomena. Atoms are deposited on the substrate in vacuum, and nanoscale structures evolve as the result of a multitude of atomistic processes. This is inherently a nonequilibrium phenomenon. Any growth scenario is governed by the competition between kinetics and thermodynamics. In thermodynamic equilibrium, detailed balance requires that all atomistic processes proceed in opposite directions at equal rate. Hence, at finite temperature, the system fluctuates around equilibrium configurations and no net growth occurs – a situation well described by statistical mechanics. The formation of nanostructures at surfaces requires nonequilibrium. A measure for the degree of nonequilibrium is the supersaturation, defined as the actual adatom/admolecule density normalized to the equilibrium adatom/admolecule density $(\rho - \rho_e)/\rho_e$. The supersaturation describes to which extent the evolving structures will be determined by the growth kinetics or by thermodynamic parameters, such as the surface and interface free energy. The larger the supersaturation, the more decisive the kinetic processes.

In a growth experiment, where atoms are deposited at a surface with a constant rate F, the diffusivity D determines the average distance l an adatom has to travel to meet another one to nucleate a new aggregate or to attach to an already formed island. In the nucleation stage at very low coverage this length decreases rapidly and eventually becomes constant, typically at coverages above a few percent of a monolayer (Brune, Roder, Boragno and Kern, 1994). In this saturation regime any further deposition will exclusively lead to the growth of existing islands. The average diffusion length l, and correspondingly the nucleation density at saturation, only depends on the ratio D:F (Pimpinelli, Villain and Wolf, 1992). The ratio of deposition to diffusion rate is thus the key quantity characterizing the growth kinetics and a measure for the supersaturation. If the deposition is slow with respect to the diffusivity, the supersaturation is low and growth takes place close to equilibrium conditions; that is, adatoms or admolecules have enough time to explore the potential energy surface to reach a minimum energy configuration. If the deposition is fast with respect to the diffusivity, the individual atomistic processes become increasingly important and the growth scenario is essentially determined by kinetics.

2.1 The hierarchy of activated motion

Of particular interest within this chapter are metal nanostructures on metal surfaces. At low substrate temperature, the growth of such a system is a prototype for the kinetically dominated growth regime. The shape and size of the nanostructures are largely determined by the competition of the active diffusion processes and can be controlled by the external parameters temperature and deposition flux and by the appropriate choice of the substrate symmetry (Röder *et al*., 1993). The central atomic processes are surface diffusion processes of single adatoms, comprising diffusion on terraces (characterized by the diffusion barrier E_d), over steps (E_s), along edges (E_e), and across corners (E_c). All these diffusion processes are thermally activated, with the respective rate depending exponentially on the potential energy barrier. To first order, these barriers scale with the local coordination; that is, terrace diffusion has a lower barrier than edge diffusion and corner crossing (Stumpf and Scheffler, 1994). Edge descend is often more costly than terrace diffusion due to an extra barrier at the edge of an island, known as the *Schwoebel–Ehrlich barrier* (Ehrlich and Hudda, 1966). For a given material system we have thus a natural hierarchy of the relevant diffusion barriers. By selective activation/freezing of a certain diffusion process we can shape the growing aggregates.

As already mentioned, the terrace diffusion barrier determines the mean free path of a diffusing adatom on the substrate surface and also on top of islands, which build up during deposition. The barrier for crossing a step fixes the average number of attempts necessary for an adatom

to descend the edge. It is the interplay between these two parameters, which determines whether an aggregate grows 2D or three-dimensionally (3D). If atoms nucleate on top of islands without having visited their edge at all, or after they have visited it too few times to descend, the aggregates grow 3D. Otherwise, the downward flux of adatoms is large enough so that no nucleation occurs on top of an island and the aggregates grow only laterally.

If the Schwoebel–Ehrlich barrier is not too large, one can always find growth conditions where the interlayer diffusion is fast enough to prevent any 3D growth. The aggregates then grow in 2D or 1D shape depending on the interplay of the various intralayer diffusion processes. Even 1D growth of aggregates can be easily initiated by choosing a substrate with an intrinsic diffusion anisotropy (Röder *et al*., 1993; Mo, Kleiner, Webb and Lagally 1991). The fcc(110) surface is such a substrate. Due to the particular structure of this surface with troughs along the [1–10] direction, diffusion is much faster along this direction than in the orthogonal [001] direction. This diffusion anisotropy and the fact that corner crossing is also anisotropic can be exploited for the growth of 1D chains (Li *et al*., 1997) (Figure 1a). Another, particularly intriguing way to promote the formation of 1D atomic chains is the use of substrate steps, as will be discussed later in this section.

On substrates with no terrace diffusion, anisotropy aggregates grow 2D with the shape determined by the competition between terrace and edge diffusion. On close-packed surfaces large compact islands can only be grown at sufficiently high temperature, where edge diffusion is active and island corners can be crossed (Röder *et al*., 1993; Michely and Comsa, 1991; Morgenstern, Rosenfeld and Comsa, 1996) (Figure 1b). At low temperature, the mobility of adatoms attached to island edges is limited or frozen and the aggregates grow in ramified island shapes (Hwang, Schroder, Gunther and Behm, 1991; Brune, Romainczyk, Roder and Kern, 1994) (Figure 1c). The metal aggregation on fcc(111) surfaces at low temperature is thus a nice model system for fractal growth in the diffusion limited aggregation scenario (Witten and Sander, 1981). The branches can be randomly ramified or grow into crystallographic well-determined directions. The latter is termed *dendritic growth* and the dominant atomistic process here is the anisotropy in the corner crossing (Brune *et al*., 1996). For square lattices, on the other hand, edge and terrace diffusion are too close in energy leading to compact island shapes even at low temperature (Zhang, Chen and Lagally, 1994).

The size of nanostructures formed in the diffusion limited regime can be controlled directly by temperature, flux, and coverage. Owing to the inherent stochastic nature of the nucleation and growth process, however, the possibility of tuning the size distribution is somewhat limited. Narrowed size distributions can be obtained by either Ostwald ripening, confined nucleation, or self-limiting processes. The nucleation regime is ideally suited to synthesize very small clusters comprising just a few atoms. The size distribution achieved here is characterized by a standard deviation roughly scaling with $<n>^{1/2}$, where n is the number of atoms. Larger particle sizes with substantially narrowed size distribution, $0.3<n>$, can be synthesized by the Ostwald ripening technique (Röder *et al*., 1993). These size distributions are, however, often sufficiently narrow to explore the size dependence of the physical and chemical properties of metallic nanostructures, such as their magnetism.

2.2 Steering and positioning

Any application of magnetic nanostructures requires the fabrication of ordered nanostructure arrays with individually

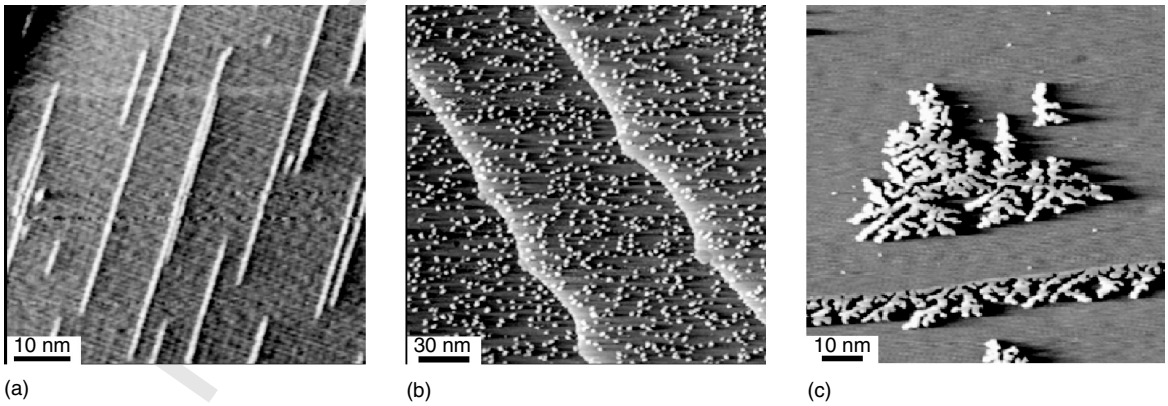

Figure 1. Atomic• architecture at surfaces by control of growth kinetics. (a) Formation of monatomic Cu chains on the anisotropic Pd(110) substrate. (b) and (c) Ag nanostructures on Pt(111); size and shape are determined by controlling the kinetic growth parameters deposition flux and temperature.

addressable units. Moreover, uniformity in position and spacing are important considerations because the properties of the nanostructures may not only depend on their size and shape but also on their mutual interactions. Thus, growth strategies need to be developed providing nearly monodisperse nanostructures, which are organized in regular arrangements.

Lateral ordering of the nanostructures can be achieved by (i) self-ordering due to mutual long-range interactions and (ii) directed growth on patterned substrates. The latter approach turned out as particularly successful for guiding nanostructure formation. The patterned surfaces serve as nanotemplates with predefined nucleation sites or energetic sinks (Brune, Giovannini, Bromann and Kern, 1998; Nötzel, 1996; Temmyo, Kuramochi, Kamada and Tamamura, 1998). With this directed self-ordering strategy, the position of each nanostructure is exactly defined by the template, thus yielding nucleation sites predictable with nanometer accuracy. Depending on the required length scale, artificially or naturally structured surfaces can be employed. Natural nanotemplates are surfaces with reconstructions (Barth, Brune, Ertl and Behm, 1990), periodic dislocation networks (Brune, Roder, Boragno and Kern, 1994), or regularly spaced steps (Hahn *et al*., 1994; Kirakosian *et al*., 2001). In these systems periodic spacings ranging from a few angstroms up to a few nanometers are provided. If larger spacings are needed, the usual top-down fabrication techniques can be applied for the fabrication of prestructured substrates (Nötzel, 1996).

Important progress in the fabrication of 2D nanostructure arrays could be made by employing substrates with dislocation networks. These dislocation networks occur naturally on some surfaces (Barth, Brune, Ertl and Behm, 1990) and can also be produced in a controlled way in thin epitaxial films (Brune, Roder, Boragno and Kern, 1994) or by wafer bonding (Leroy, Eymery, Gentile and Fournel, 2002). Typical periodicities range between 2 and 20 nm. The dislocations lines are in general found to be repulsive toward diffusing atoms (Brune, Giovannini, Bromann and Kern, 1998; Fischer *et al*., 1999), while dislocation elbows can act as sinks for mobile atoms (Chambliss, Wilson and Chiang, 1991). For a well-defined set of growth parameters, the adatoms are, therefore, in the first case confined within the dislocation network unit cells, exactly nucleating one island per unit cell. In the second case, islands preferentially nucleate at the attractive defects. These techniques have successfully been applied in the growth of metal or semiconductor nanostructure arrays and even magnetic nanopillars (Fruchart, Klaua, Barthel and Kirschner, 1999). A valuable side effect of the nucleation and growth on such patterned substrates is the typically enhanced size uniformity. In this case, the size distribution becomes binominal and the size uniformity is determined by the statistical fluctuations in the deposition process. As the homogeneity increases with the size of the atom collecting area, the monodispersity becomes better with increasing island distance (Brune, Giovannini, Bromann and Kern, 1998).

As mentioned earlier, vicinal, that is, regularly stepped, surfaces can serve as natural nanotemplates for the self-organized growth of 1D nanoarrays. The step edges act as preferential nucleation sites for the deposited material due to the increased coordination with respect to the terrace sites. A row-by-row decoration of the steps can be achieved if (i) the terrace mobility is high enough that all adatoms can reach the steps and (ii) the mobility of the atoms once attached to the steps is still sufficient to ensure 1D nucleation and growth (Gambardella *et al*., 2000). At appropriate deposition temperatures, the width of the adlayer chains can be changed discretely from monatomic to diatomic, triatomic and so on, simply by controlling the total coverage. Perfect 1D nanotemplates are for example, the (557) surface of Si and the (997) surface of Pt, which had been proven to show highly ordered step structures (Hahn *et al*., 1994; Kirakosian *et al*., 2001). As an example, the Pt(997) surface composed of (111) oriented terraces of 20.2 Å in width, separated by monatomic steps, is shown in Figure 2(a). The regular step ordering is mediated by the repulsive step–step interactions, which suppress step meandering. As examples for nanotemplate supported growth, arrays of 1D Co and Fe chains fabricated on Pt(997) will be discussed within this chapter (see Figure 2b and inset in Figure 8a).

3 MAGNETISM OF ZERO- AND ONE-DIMENSIONAL STRUCTURES

3.1 Magnetic atoms on nonmagnetic substrates

In this chapter, we are concerned with fundamental issues that govern the intrinsic magnetic properties of low-dimensional metal systems fabricated by molecular beam epitaxy on nonmagnetic substrates. We define as *intrinsic* those properties that depend on atomic scale magnetism and crystalline structure, such as the magnetic moment, the magnetocrystalline anisotropy, and magnetic order, as opposed to the *extrinsic* properties that depend on the microstructure and magnetostatic interactions (Kronmüller, 2003; Skomski and Coey, 1999). The main focus will be on 0D and 1D systems, where the influence of size and dimensionality effects on the intrinsic magnetization parameters is largest. For a thorough treatment of 2D systems such as magnetic thin films and multilayers, we refer to the extensive monographs published on the subject (Gradmann, 1993; Schneider and Kirschner, 2000; Bland and Heinrich, 2005) and to •other chapters of this handbook.

Q3

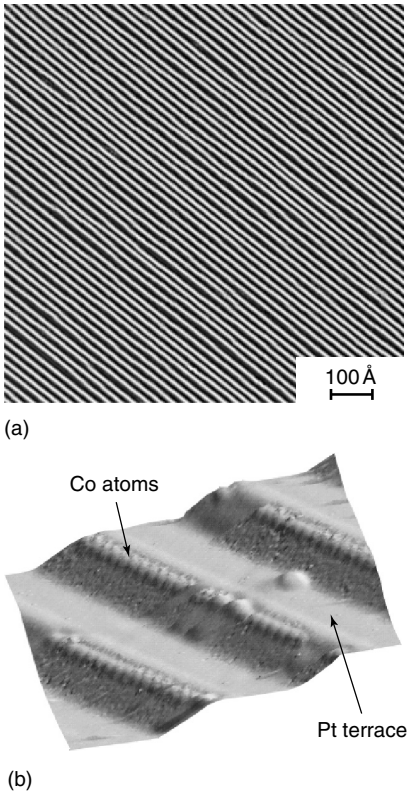

Figure 2. (a) The STM image of a Pt(997) surface shows (111)-oriented terraces of identical width, separated by monatomic steps. The high degree of order makes this substrate an ideal nanotemplate for nanostructure fabrication. (b) Formation of monatomic chains of Co atoms by substrate step decoration.

Q4

The fabrication of magnetic nanostructures and thin films by •MBE methods is typically initiated by the deposition of magnetic atoms from the vapor-phase onto a nonmagnetic substrate, as discussed in the preceding text. A first point of fundamental and practical interest, in this context, is the extent to which the local magnetic moment of a transition metal impurity is modified by the interaction with the supporting substrate. The role played by magnetic/nonmagnetic interfaces in determining the magnetization and particularly the anisotropy fields in ultrathin films has been widely investigated in the past (Gradmann, 1993; Sander, 2004). With the aim of controlling the magnetic behavior of structures with ever reducing dimensions, however, our knowledge must progress toward the atomic size level. Identifying and distinguishing local substrate-impurity hybridization effects from coordination and magnetoelastic effects in thin films, for instance, provide useful guidelines to tailor the intrinsic magnetization parameters in finite-sized supported particles, optimize sensitive interface properties that govern electron transport in magnetoelectronic devices (Jansen and Moodera, 1998), and test current theoretical models of low-dimensional magnetic systems (Blügel, 2007).

Most transition metal atoms in the gas phase possess large spin (m_S) and orbital (m_L) magnetic moments due to the incomplete filling of the d-shell and the atomic correlation effects exemplified by the Hund's rules. In the solid state, electron delocalization and crystal field effects compete with intra-atomic Coulomb interactions causing a substantial or total decrease of m_S and quenching of m_L. Theoretical calculations, however, predict such effects to be strongly reduced at surfaces owing to the decreased coordination of transition metal impurities (Blügel, 2007; Stepanyuk *et al*., 1996; Nonas *et al*., 2001). As a case experimental system, we consider the magnetic properties of Co. As free atom in the ground state d^7 configuration, Co displays significant spin and orbital magnetism with $m_S = m_L = 3\ \mu_B$, and Brillouin-like isotropic magnetization (Figure 3a). In the bulk hexagonal close-packed structure Co is a strong ferromagnet with $m_S = 1.52$ and $m_L = 0.15\ \mu_B$ and exhibits a fairly large •MCA compared to bulk Fe and Ni with a uniaxial anisotropy energy constant $K = 0.05$ meV per atom (Bonnenberg, Hempel and Wijn, 1986).

Q5

Once deposited onto a metal surface, we expect the magnetic moment of Co atoms to vary according to the degree of d-orbital hybridization with the conduction electron

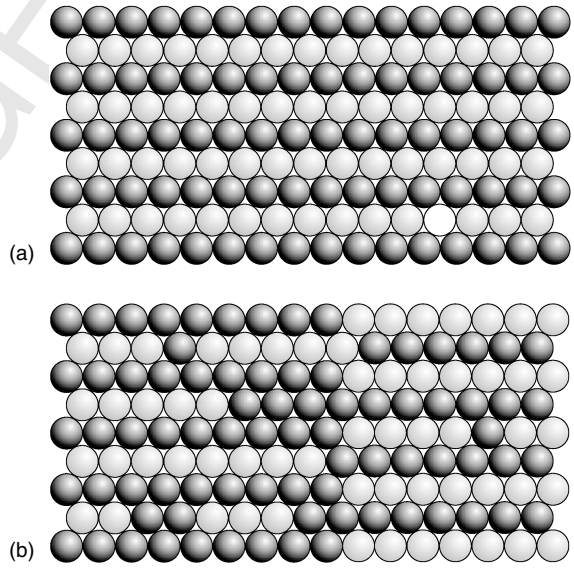

Figure 3. (a) Spin and orbital magnetic moment of a gas phase Co atom as given by the Hund's rules for the d^7 electronic configuration. The magnetic anisotropy energy equals zero due to the spherical symmetry of the system. The isotropic magnetization is represented by a Brillouin function for the d^7 state calculated at $T = 5.5$ K. (b) Spin and orbital magnetic moment and magnetic anisotropy energy of an individual Co atom deposited on the Pt(111) surface. The anisotropic magnetization is measured at $T = 5.5$ K by recording the XMCD intensity at the Co L_3 edge as a function of applied field in the easy (out-of-plane, filled circles) and hard (in-plane, empty circles) direction.

states of the substrate (Gambardella *et al*., 2002b; Song and Bergmann, 2001). This will depend on the reduced number of neighbors around the impurity as well as on the host band structure, similar to dilute alloys with nonmagnetic metals (Mydosh and Nieuwenhuys, 1980). In dealing with surface impurities, the experimental challenge lies in probing extremely reduced amounts of magnetic atoms (typically the order of 10^{14} atoms cm^{-2} or less, deposited at cryogenic temperature to avoid cluster formation) on a macroscopic metal surface with nonnegligible para- or diamagnetic response. To achieve the required element-specific sensitivity, the method of choice is the absorption of circularly polarized light in the soft X-ray range, described in Chapter •XXX of this volume. The lineshape of the X-ray absorption spectra (XAS) at the $L_{2,3}$ edges of 3d transition metals ($2p^6 3d^n$ to $2p^5 3d^{n+1}$ excitations) contains information about the electronic configuration of the impurities (van der Laan and Thole, 1991). Simultaneously, as the X-ray absorption cross-section depends on the orientation of the spin and orbital moment of the 3d electrons relative to the X-ray polarization direction, magnetic sensitivity is achieved by taking the difference of the XAS spectra for parallel (I_+) and antiparallel (I_-) alignment of the X-ray polarization with respect to the sample magnetization. The X-ray magnetic circular dichroism (XMCD) spectra obtained in this way allow to identify the magnetization direction and strength of a given element (Stöhr, 1999), and to estimate quantitatively m_S and m_L by means of the so-called *XMCD sum rules* (Thole, Carra, Sette and Van der Laan, 1992; Carra, Thole, Altarelli and Wang, 1993; Chen *et al*., 1995).

As an example of a strongly interacting substrate we present data obtained for the Pt(111) surface. The XAS of isolated Co impurities deposited in ultra-high-vacuum on Pt(111) (Figure 4a) reveals broad features typical of Co metal (Figure 4b) that are drastically different from the XAS calculated for the atomic d^7 configuration (Figure 4c) and observed in the vapor-phase (Martins, Godehusen, Richter and Zimmermann, 2003). The spectrum of Co/Pt(111) differs also from that of Co impurities deposited on free-electron metals, such as K, where the narrow XAS multiplet structure indicates that the Co ground state has d^8 atomic-like character (Figure 4c). In the latter case s-d charge transfer takes place, but the Co 3d states remain essentially localized with both m_S and m_L close to the integer Hund's rule limit (Gambardella *et al*., 2002b). On a transition metal surface such as Pt, on the other hand, the electron density is much larger and the impurity 3d-states can hybridize with both the s- and d-states of the substrate. This leads to a strong reduction of m_S and m_L compared to the vapor-phase. Owing to its reduced coordination, the impurity magnetic moment is nonetheless significantly enhanced with respect to 2D films (Tischer *et al*., 1995; Weller *et al*., 1995), supported

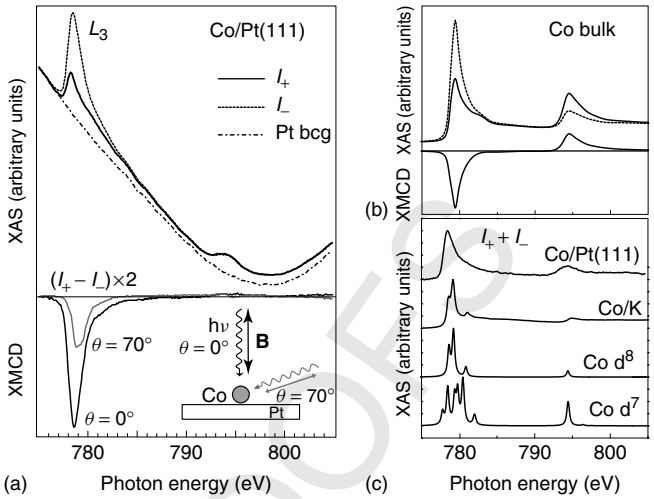

Figure 4. (a) $L_{3,2}$ XAS spectra of Co impurities (0.03 ML) deposited on Pt(111) recorded at $T = 5.5$ K, **B** = 7 T with parallel (I_+) and antiparallel (I_-) alignment of the photon helicity with respect to **B** at an angle $\theta = 0°$ relative to the surface normal. The Co XAS appears superimposed on the background signal of the Pt substrate (dotted line). The XMCD ($I_+ - I_-$) is shown at the bottom for $\theta = 0°$ and 70°. (b) XAS and XMCD spectra of bulk Co. (c) Comparison between the total XAS ($I_+ + I_-$) after background subtraction for Co impurities on Pt(111), Co impurities on a K film, and the calculated XAS for atomic-like d^8 and d^7 configurations.

nanoparticles (Dürr *et al*., 1999; Koide *et al*., 2001), and 1D atomic chains (Gambardella *et al*., 2002a). According to the XMCD sum rules, the vanishing intensity of the XMCD at the L_2 edge in Figure 4(a) compared, for example, to Figure 4(b) indicates that the largest enhancement is that of the orbital component of the magnetic moment, for which we get $m_L = 1.1 \pm 0.1\ \mu_B$.

The presence of strong orbital magnetism allows unusually large MCA through the spin-orbit interaction (Bruno, 1989; Dürr *et al*., 1997). The MCA energy can be determined by means of XMCD by measuring the magnetization of the Co atoms in an external field applied along different directions with respect to the substrate normal, as shown in Figures 3(b) and 4(a). The solid lines represent fits of the data by means of numerical integration of the equation that describes the impurity magnetization in the presence of the applied field and uniaxial anisotropy energy (Gambardella *et al*., 2003). For isolated impurities we have $K = 9.3 \pm 1.6$ meV per atom, a remarkable value compared to typical systems with high MCA such as $SmCo_5$ ($K = 1.8$ meV per Co atom Weller and Moser, 1999), Co/Pt and Co/Au multilayers ($K \sim 0.3$ meV, Nakajima *et al*., 1998; Weller *et al*., 1995). Different effects combine in establishing the giant MCA of Co atoms on the Pt surface. The main point is the reduced atomic coordination, which results into narrow 3d-electron bands localized at the impurity sites with

augmented spin-orbit interaction due to the increase of the local density of states near the Fermi level (Bruno, 1989; Dürr *et al*., 1997) and 3d–5d hybridization. Further, the Pt atoms close to Co are magnetically polarized and present an additional MCA due to the strong spin-orbit coupling of the Pt 5d-states. Theoretical calculations indicate the first effect to be dominant (Gambardella *et al*., 2003) although the two contributions cannot be separated experimentally because of exchange coupling between the Co and Pt magnetic moments.

3.2 Magnetic moment and magnetic anisotropy in finite-sized particles

It is well-known that size effects in metal particles containing a nonnegligible ratio of surface to volume atoms influence the saturation magnetization and MCA properties in cluster beams (Billas, Chatelain and de Heer, 1994; Apsel, Emmert, Deng and Bloomfield, 1996; Knickelbein, 2001) as well as in surface-supported systems (Dürr *et al*., 1999; Edmonds *et al*., 1999; Koide *et al*., 2001; Ohresser *et al*., 2001; Lau *et al*., 2002; Rusponi *et al*., 2004; Bansmann *et al*., 2005). Such effects become dominant as we reach down to nanometer dimensions. In this critical size regime, key questions are: how MCA evolves from single atoms to finite-sized particles; how it correlates to atomic magnetic moments; and how both depend on the details of the atomic coordination. By exploiting the energetic hierarchy and temperature dependence of surface diffusion and nucleation processes, the bottom-up approach described in Section 2 allows us to study the development of the magnetization and MCA in magnetic particles constructed on a nonmagnetic substrate starting from isolated magnetic atoms and increasing the particle size almost in an atom-by-atom fashion. Following the previous section, we consider monolayer Co particles grown on Pt(111) as model system. While m_S is expected to vary in a fairly restricted range between 2.1 and 2.2 μ_B for an individual impurity (Gambardella *et al*., 2003; Lazarovits, Szunyogh, Weinberger and Újfalussy, 2003) to 1.8–1.9 μ_B for a continuous 2D layer (Wu, Li and Freeman, 1991), since the majority spin band is almost filled in all cases, m_L is shown to be much more sensitive to changes in the atomic coordination, reflecting its closer link with the symmetry and relative filling of the d-orbitals. Figure 5(a) reports the progressive quenching of m_L as a function of average particle size $\overline{n}$. Remarkably, the largest changes of m_L are observed for the smallest particles: for $\overline{n} = 3$ and 4 atoms, m_L has already reduced to 0.78 and 0.59 μ_B, respectively. The MCA energy, due to its spin-orbit origin (Bruno, 1989; Dürr *et al*., 1997), is found to be strongly correlated to the decrease of m_L (Figure 5b). Similar to m_L, drastic changes of K are

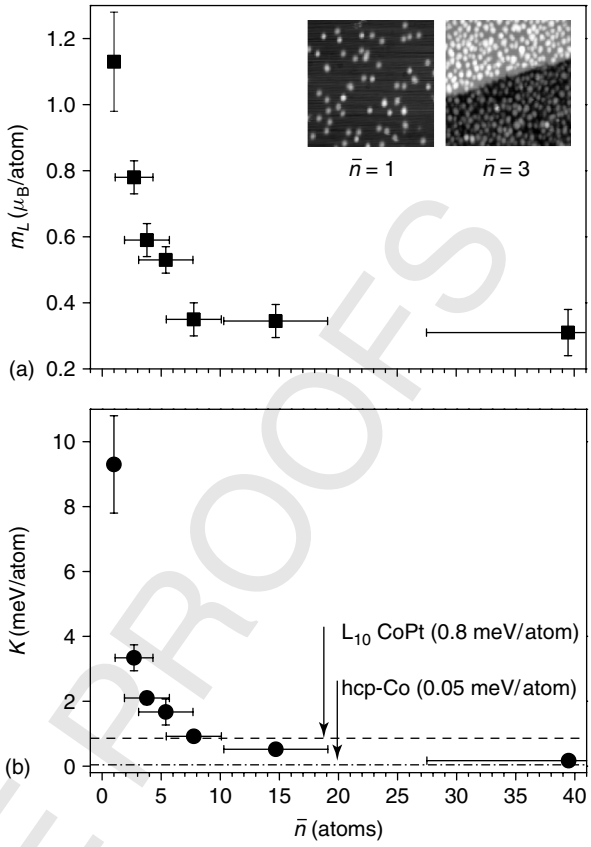

Figure 5. (a) Orbital magnetic moment of monolayer Co nanoparticles deposited on Pt(111) as a function of their average size measured along the easy magnetization direction ($\theta = 0^\circ$). (b) Magnetic anisotropy energy as a function of average particle size. The dashed and dashed-dot lines indicate the magnetic anisotropy energy per Co atom of the CoPt $L1_0$ alloy and *hcp*-Co, respectively. The error bars on the horizontal scale in (a) and (b) represent the standard deviation of the size distribution as determined by STM. The inset shows 180 × 180 Å^2 STM images of Co impurities and particles with average size $\overline{n} = 1 \pm 0.1$ and 3 ± 1 atoms.

observed for one-atom variations of the atomic coordination: for $\overline{n} = 3$ atoms, $K = 3.3$ meV amounts to only 30% of the individual impurity value, while already for $\overline{n} > 10$, K drops below the anisotropy energy of the equi-atomic CoPt alloy.

The trend evidenced in Figure 5(b) shows that a huge gain in MCA with respect to bulk or 2D films can be obtained by reducing the size of magnetic particles to a few tens of atoms or less on suitable substrates. Whereas this holds on a per atom basis, it is obvious that the overall stability of the particle magnetization is governed by the sum of the atomic MCA contributions. As more atoms are assembled together to fabricate particles with a large total magnetic moment and total MCA strong enough to stabilize ferromagnetic behavior against thermal fluctuations, this gain is countered by the decrease of K with increasing $\overline{n}$. The problem, however, can be circumvented by noting that the atomic coordination

rather than the absolute particle size is the key parameter that governs the magnitude of K, m_L, and m_S. Nanostructures where the shape and composition are tuned so as to control the coordination of the magnetic atoms and maximize useful interface effects, such as in nanowires (Gambardella *et al*., 2002a, 2004) and core-shell particles (Rusponi *et al*., 2004), offer very interesting opportunities to exploit the effects highlighted in this section.

3.3 Magnetic moment and magnetic anisotropy in 1D atomic chains

The dependence of intrinsic magnetization properties on the atomic coordination gives rise to a very diverse magnetic behavior in metal systems that span the 1D–2D limit. As described in Section 2, epitaxial growth on stepped surfaces can be employed to fabricate arrays of nanowires whose thickness and separation are independently adjusted by controlling the coverage and vicinal angle of the substrate. A large number of parallel nanowires are obtained using this method, which allows to use spatially integrating techniques with magnetic sensitivity such as Kerr magnetometry and XMCD. This approach was first explored by Elmers *et al*. (1994) and Pratzer *et al*. (2001) in the study of Fe monolayer stripes grown on stepped W(110). This system presents in-plane anisotropy, scaling of the ordering temperature of each Fe stripe typical of a finite-sized 2D Ising lattice, and a relaxation-free ferromagnetic phase transition due to dipolar coupling across adjacent stripes (Hauschild, Elmers and Gradmann, 1998). Shen *et al*. (1997a,b) found a pronounced temperature- and time-dependent magnetic relaxation for mono- and bilayer Fe stripes on stepped Cu(111) with out-of-plane anisotropy, due to the formation of 1D Ising-coupled spin blocks. Fe stripes on vicinal Pd(110) also present perpendicular anisotropy (Li *et al*., 2001), but the magnetization was found to be time-independent. Recently, Co wires of monatomic thickness have been grown at the step edges of Pt(997) (Figure 2) (Gambardella *et al*., 2000, 2002a) and along the close-packed atomic rows of Pd(110) (Yan *et al*., 2005).

In the limit of atomically thin metal chains, *ab initio* electronic calculations predict large exchange splittings and strongly increased m_S and m_L relative to those of the bulk and 2D monolayers (Weinert and Freeman, 1983; Komelj, Ederer, Davenport and Fähnle, 2002; Ederer, Komelj and Fähnle, 2003; Spisák and Hafner, 2002; Lazarovits, Szunyogh and Weinberger, 2003; Shick, Máca and Oppeneer, 2004) as well as MCA energies exceeding 1 meV per atom (Lazarovits, Szunyogh and Weinberger, 2003; Hong and Wu, 2003, 2004; Újfalussy *et al*., 2004; Shick, Máca and Oppeneer, 2004). Similar to the case of individual impurities, these variations are attributed to the reduced overlap between the d-orbitals in 1D structures. Angle-resolved photoemission experiments on Co monatomic chains grown along the step edges of Pt(997) corroborate the prediction of large exchange splitting of the Co 3d states (2.1 eV Dallmeyer *et al*., 2000) compared to thin films (1.4–1.9 eV) and bulk Co (1.4 eV) (Schneider *et al*., 1990; Clemens *et al*., 1992), suggesting that m_S is of the order of 2 μ_B (Himpsel, Ortega, Mankey and Willis, 1998). XMCD measurements on the same system show that $m_L = 0.68$ μ_B in the monatomic limit, more than twice the value found for a Co monolayer on Pt(997), but drops already to 0.37 μ_B per atom in chains with biatomic thickness (Gambardella *et al*., 2002a). Such values can be rationalized within the trend framed in the previous section, where the average coordination among Co atoms determines large differences of m_L. On the basis of Figure 5(a), for instance, we expect $m_L \approx 0.7$ μ_B per atom for $\overline{n} = 3$, that is, for Co atoms with an average of two Co neighbors, which corresponds to the Co coordination in the monatomic chains.

The sensitivity to the transverse structure of the chains concerns also the orientation of the easy axis and the magnitude of the MCA (Gambardella *et al*., 2004). In Figure 6, we report the magnetization of Co chains with different thickness measured in the plane perpendicular to the chain axis. The magnetization, measured near-remanence at angles θ with respect to the (111) direction, is typical of a uniaxial system and presents a sinusoidal behavior whose maximum indicates the orientation of the easy axis. In the monatomic chains the easy axis is canted toward the step-up direction due to the reduced symmetry at the Pt step edges, an effect that has been reproduced by first principles relativistic calculations (Újfalussy *et al*., 2004; Shick, Máca and Oppeneer, 2004). With increasing chain thickness unusual oscillations of the easy magnetization direction are observed in the plane perpendicular to the chains (Gambardella *et al*., 2004). The easy axis rotates abruptly from $\theta = +46^\circ$ in the monatomic chains to -60° in the biatomic chains and reverses back toward the surface normal in the monolayer limit as shown in Figure 6. The analysis of the easy and hard magnetization curves reported in Figure 7 reveals further that the magnitude of the MCA has a nonmonotonic behavior with chain thickness. In the monatomic limit $K = 2$ meV per atom at $T = 45$ K, a value enhanced by 1–2 orders of magnitude compared to 2D films (Gradmann, 1993), but in line with expectations based on theoretical calculations (Dorantes-Dávila and Pastor, 1998; Félix-Medina, Dorantes-Dávila and Pastor, 2002; Lazarovits, Szunyogh and Weinberger, 2003; Hong and Wu, 2003, 2004; Újfalussy *et al*., 2004; Shick, Máca and Oppeneer, 2004) and the experiments presented in the previous section. Given that in nanoparticles K is a rapidly decreasing function

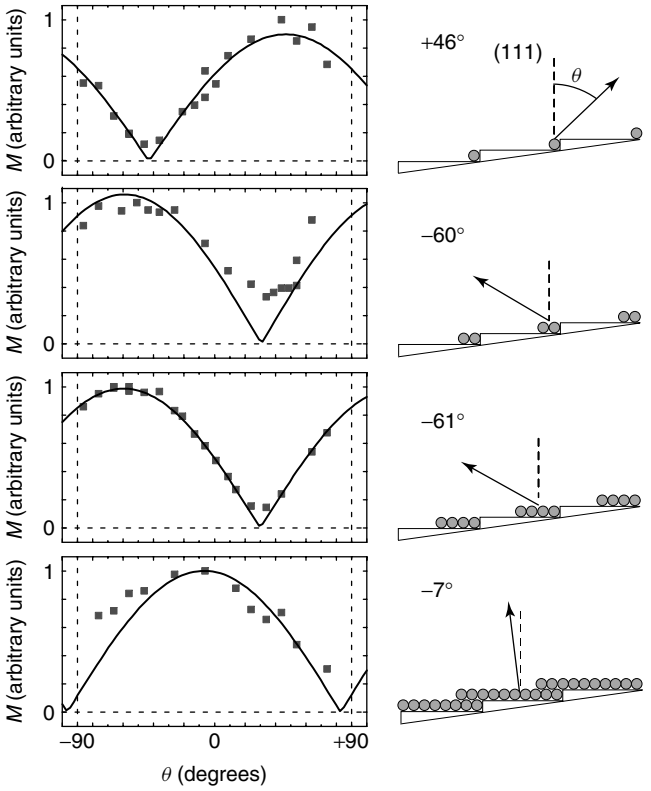

Figure 6. Near-remanence magnetization of Co chains deposited on Pt(997) as a function of the angle θ between the incident photon beam and (111) direction in the plane perpendicular to the chain axis. The data points represent the XMCD signal at the L_3 Co edge. The solid lines fit a $|\cos(\theta - \theta_0)|$ behavior as expected for uniaxial anisotropy. The diagrams indicate the chain thickness and the easy axis direction given by the maximum of the $|\cos|$ function.

of the local coordination (Figure 5b), it is not surprising that K reduces to 0.33 meV per atom in the biatomic chains. In triple chains, however, K shows a significant and unexpected increment, upto 0.45 meV per atom, before decreasing again in the monolayer limit. These oscillations as well as the sign inversion of the MCA represented by the rotation of the easy axis appear to be due to thickness-dependent changes in the electronic band structure of the chains rather than to extrinsic (dipolar) effects (Gambardella *et al*., 2004; Vindigni *et al*., 2006), as shown also by tight binding calculations of both free-standing and Pd-supported Co chains one to three atoms thick (Dorantes-Dávila and Pastor, 1998; Félix-Medina, Dorantes-Dávila and Pastor, 2002). Reducing the dimensions of a magnetic layer down to 1D, therefore, reveals a nontrivial magnetic behavior and new opportunities to tune the magnetization properties in metal nanostructures. Examples include the high anisotropy of the 1D-modulated FePt surface alloy presented in Section 4 and the emergence of magnetism in chains of 4d and 5d metals (Bellini, Papanikolaou, Zeller and Dederichs, 2001; Spisák and Hafner, 2003; Rodrigues, Bettini, Silva and Ugarte, 2003).

3.4 Magnetic order in 1D atomic chains

The dimensionality of a magnetic lattice is known to affect not only local properties such as the magnetic moments and MCA but also its thermodynamic properties and in particular order–disorder magnetic phenomena. Ferromagnetism in 2D films is typically more sensitive to temperature-induced fluctuations of the magnetization compared to 3D systems due to the reduced number of atoms contributing to the total exchange interaction (Gradmann, 1993; Schneider and Kirschner, 2000; Poulopoulos and Baberschke, 1999). In the well-known case of the Heisenberg and Ising models, the thermodynamic limit of a 1D spin chain of infinite length is characterized by the absence of long-range magnetic order at any nonzero temperature (Ising, 1925; Mermin and Wagner, 1966; Bruno, 2001). In the past, quasi-1D insulating inorganic crystals have been investigated as Heisenberg model systems to test predictions about magnetism in 1D (De Jongh and Miedema, 1974; Hone and Richards, 1974); typical examples include tetramethylammonium copper and manganese chloride compounds, where Cu^{2+} and Mn^{2+} ions couple ferromagnetically or antiferromagnetically, respectively, along weakly interacting linear chains separated by intervening nonmagnetic complexes (Dingle, Lines and Holt, 1969; Landee and Willett, 1979; Dupas, Renard, Seiden and Cheikh-Rouhou, 1982). More recently, the synthesis of molecular ferri- and ferromagnetic chainlike compounds containing magnetically anisotropic ions has allowed to realize 1D Ising model systems where the absence of permanent magnetic order is accompanied by the slow relaxation of the magnetization (Caneschi *et al*., 2001; Bogani *et al*., 2004; Clérac, Miyasaka, Yamashita and Coulon, 2002; Lescouëzec *et al*., 2003) as predicted by Glauber more than 40 years ago (Glauber, 1963). The fabrication of 1D chains of magnetic atoms deposited on a nonmagnetic substrate with the methods described in Section 2 opens up the possibility of extending the investigation of 1D magnetic behavior to metal systems.

The magnetic response of a set of monatomic Co chains at $T = 45$ K (Figure 7a) reveals zero remanent magnetization and the absence of long-range ferromagnetic order. The shape of the magnetization curves, however, indicates the presence of short-range order, that is, of significant interatomic exchange coupling in the chains (Gambardella *et al*., 2002a; Vindigni *et al*., 2006). The observed behavior is that of a 1D superparamagnetic system, that is, a system composed by segments, or spin blocks, each containing N exchange-coupled Co atoms, whose resultant magnetization orientation is unstable due to thermal fluctuations. Fitting

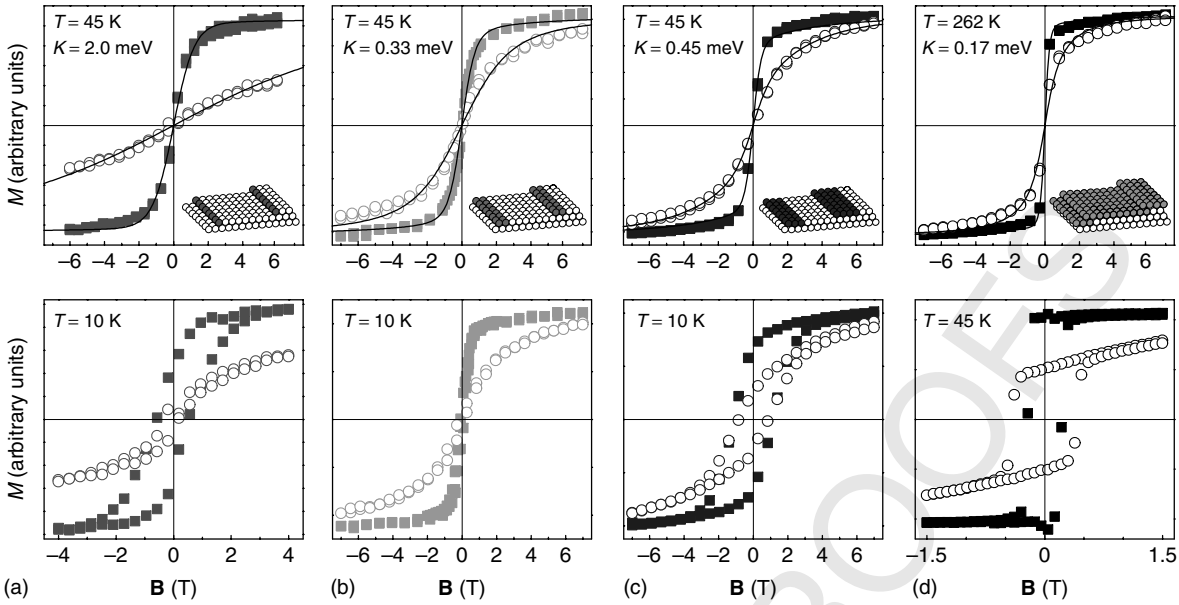

Figure 7. Magnetization of (a) monatomic Co chains, (b) double chains, (c) triple chains, (d) 1.3 monolayers in the easy (filled squares) and hard direction (empty circles). The data points represent the XMCD intensity at the Co L_3 edge as a function of applied field. The solid lines in the top panels are fits of the data in the superparamagnetic regime as described in Gambardella *et al*. (2002a).

the magnetization curves assuming uniaxial MCA and a Boltzmann distribution of the energy states accessible by the system (solid lines) gives the average value $N = 15$ atoms, smaller than the average length of the Co chains, which is estimated to be about 80 atoms from the extension of the atomically straight sections of the Pt steps that act as deposition template. A simple argument of Landau (Landau and Lifshitz, 1959) shows that this result does not contradict the predicted absence of magnetic order in 1D by spin lattice models as long as $N \leq e^{2J/kT}$, where J represents the exchange interaction among adjacent spins ($J \approx 15$ meV Frôta-Pessoa, Muniz and Kudrnovský, 2000; Pratzer *et al*., 2001). However, by lowering the sample temperature below 15 K, we observe a transition to a ferromagnetically ordered state with long-range order and finite remanence at zero field (Figure 7a, bottom panel). This order transition is not dominated by the exchange interaction as in 3D crystals, but rather by the presence of large MCA energy barriers that effectively inhibit the spin fluctuations that lead to the zero remanence thermodynamic limit expected for 1D systems. Below the blocking temperature the magnetization of each spin segment aligns along the common easy axis direction and the system becomes ferromagnetic on a macroscopic scale. Long-range order in 1D metal chains therefore appears as a metastable state, thanks to slow magnetic relaxation. It is interesting to note that as the system evolves toward a 2D film and the number of exchange-coupled Co atoms increases (Figure 5b), we would expect a stronger tendency toward magnetic order. Contrary to expectations, however, in the biatomic chains we observe vanishing long-range magnetic order even at low temperature (Figure 5b). In this case, the tendency toward order is counteracted by the drastic reduction of the MCA energy per Co atom. Paradoxically, therefore, the 1D character of the monatomic chains favors rather than disrupts ferromagnetic order owing to the minimal coordination of the Co atoms and related enhanced MCA.

4 TOWARD TWO-DIMENSIONAL MAGNETIC STRUCTURES

It is commonly believed that, of all 3d elements, the magnetism of Fe based nanostructures depends the most on the local atomic environment and the interaction with the underlying substrate. This is due to the fact that Fe is a 'borderline ferromagnet' with an exchange interaction sensitively depending in magnitude and sign •on the structure on the atomic level (Pajda *et al*., 2000, 2001; Bruno and Sandratskii, 2005). Being a weak ferromagnet, the presence of empty states at the Fermi energy in the minority and majority subband results in a complex dependency of the magnetic properties on the d-band width and occupation, which are controlled by the local atomic coordination. As constructed from Hund's rules, free Fe atoms in the $3d^6 4s^2$ ground state possess spin- and orbital moments of $m_S = m_L = 2\ \mu_B$. In the bulk phase the electron hybridization quenches the orbital moment to $m_L = 0.1\ \mu_B$ (Chen

Q7

et al., 1995). Low-dimensional Fe nanostructures at surfaces are useful to address open questions about the magnetic anisotropy on the atomic level. Of particular interest, in the following sections, are changes in the magnetism with dimensionality during the crossover from 1D Fe monatomic wires to a 2D Fe or FePt monolayer. As seen in Section 3, the interaction with the substrate has also a decisive influence on the magnetism and can be exploited to tune many of the magnetic properties in low-dimensional structures. The traits of Pt – large Stoner-enhanced susceptibility together with the strong spin-orbit coupling of the 5d states – make it an attractive substrate material for magnetic nanostructures. In contact with 3d magnetic elements Pt acquires a sizable magnetic polarization and gives an important contribution to the magnetocrystalline anisotropy. The role of the substrate will be discussed in the following for all investigated Fe structures, but becomes most apparent for FePt surface alloy layers.

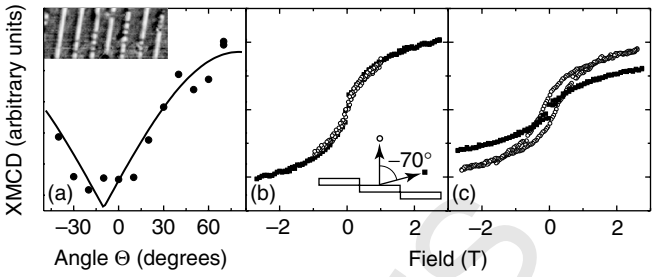

Figure 8. XMCD measurements taken at the Fe L_3 absorption edge as a function of field at 10 K of (a) 0.13 ML Fe (monatomic Fe chain) as a function of polar angle Θ in a constant magnetic field of 1 T. The solid line is a $|\cos(\Theta - \Theta_0)|$ – fit to the data. (b) Hysteresis loops of 0.38 ML Fe (3 atomic stripe), and (c) 0.8 ML (6 atomic stripe). Measurements are taken along the surface normal (o) and under a polar angle of 70° in the direction perpendicular to the step edges (■). A reorientation of the preferred magnetization axis from in-plane perpendicular to the step edges (a) toward perpendicular to the surface (c) occurs with increasing Fe coverage. Inset: STM image of 0.11 ML Fe/Pt(997) showing the wire formation by step decoration.

4.1 Fe on Pt – from atomic chains to layered films

Since the early experiments on Fe stripes of finite width prepared on W(110) by Elmers *et al*. (1994) 1D linear Fe nanostructures have been prepared successfully also on vicinal Au (Kawagoe, Sogabe, Kondoh and Narusawa, 1998; Shiraki, Fujisawa, Nantoh and Kawai, 2004, 2005), Cu (Shen *et al*., 1997b; Boeglin *et al*., 2002; Fruchart *et al*., 2004) or Si substrates (Lin *et al*., 2001), on reconstructed Ir surfaces (Klein, Schmidt, Hammer and Heinz, 2004), or by organic patterning (Ma *et al*., 2004). Also on the vicinal Pt(997) surface, Fe shows a strong tendency toward substrate step decoration. Fe atoms arrange themselves to segments of atomic chains at the step edges at growth temperatures between 200 K and 450 K (Lee, Sarbach, Kuhnke and Kern, unpublished). Extended monatomic chains of Fe are thus formed at a coverage of $\Theta_{Fe} = 0.13$ ML, •limited in length only by kinks at step edges or by point defects. The wire formation is, hence, in analogy to the Co chains described in the previous chapter. After complete step decoration, the growth proceeds in the step flow mode until the first Fe monolayer is completed. The layer-wise growth is promoted by the presence of the dense array of substrate steps (Lee, Sarbach, Kuhnke and Kern, unpublished).

The evolution of the magnetic anisotropy of Fe stripes with increasing stripe width shows distinctive differences to the Co chains presented in the previous section. The XMCD data in Figure 8 reveal that for a coverage corresponding to 1 atomic row in (a) the preferred magnetization direction is perpendicular to the wire axis, but close to the substrate surface. With increasing coverage the magnetization axis reorients gradually toward the out-of-plane direction. For a coverage corresponding to 3 atomic rows in (b) no distinctive difference between out-of-plane and in-plane magnetization loops is visible, while for 6 rows in (c) the easy magnetization axis points out of the surface plane. For all samples investigated, the in-plane axis along the wire represented the hard magnetization direction. The comparison with Co allows for two important conclusions: (i) In both systems a preferred magnetization perpendicular to the chain axis is found. Whereas Co chains exhibit an oscillatory reorientation of the magnetization with increasing width, Fe chains rather show a gradual transition from in-plane to out-of-plane magnetization. Complete Fe and Co monolayers have an easy axis close to the sample normal. (ii) The MCA in Fe single atomic chains is 0.56 meV per atom, as determined from fits to angular dependent hysteresis loops. This value is significantly enhanced with respect to the Fe bulk value, but smaller compared to Co chains of equal thickness (∼2 meV per atom, see previous section). The MCA of monatomic Fe chains is not sufficient to stabilize remanent magnetization at 10 K, in contrast to Co. In both systems the enhanced MCA goes along with an increase of the orbital moment per atom with respect to bulk, as will be discussed later in this section.

Ab initio electron theory suggests strong similarities in the physics of Co and Fe monatomic chains (Ederer, Komelj and Fähnle, 2003; Shick, Máca and Oppeneer, 2005). The observed ferromagnetic ordering and the enhanced magnetic moments have been predicted theoretically for free and supported atomic chains of Fe (Spisák and Hafner, 2002; Dorantes-Dávila and Pastor, 1998; Lazarovits, Szunyogh, Weinberger and Újfalussy, 2003; Jin, Kim and Lee, 2004). The easy magnetization axis is found perpendicular to the

wire axis in all published calculations, as a result of strong Fe–Fe bonds along the chains and the resulting intrachain exchange coupling in this direction. However, the calculated tilt angle of $+30^{\circ}$ to the surface normal (Shick, Máca and Oppeneer, 2005) is in contrast to our experiment. The calculated tendency of the magnetization to be perpendicular to the Fe–Fe bonding direction may explain the reorientation of the easy axis toward out-of-plane when increasing the Fe coverage above the monochain coverage. Already for chains of 2 atoms in width the intrawire coupling strength perpendicular to the wire axis is of the same order of magnitude as found along the wire (Lazarovits, Szunyogh, Weinberger and Újfalussy, 2003). The intra- and interchain magnetic coupling exceed the dipolar interaction by 2 orders of magnitude and thus dominate the magnetic anisotropy (Spisák and Hafner, 2002). The dipolar interaction would favor ferromagnetically ordered arrays of wires with an in-plane magnetization direction along the wires, which is clearly not observed.

It is important to note that the interaction with the substrate affects the MCA of the wires. This can be seen from a comparison of the experimental data with calculations on free wires which show preferred magnetization *along* the wire axis (Dorantes-Dávila and Pastor, 1998). The role of the substrate is to contribute its spin-orbit coupling to the whole system, thus increasing the total MCA (Dorantes-Dávila and Pastor, 1998), to alter the density of states at the Fermi level (Lazarovits, Szunyogh, Weinberger and Újfalussy, 2003), and possibly to establish interchain coupling by RKKY interaction via intervening substrate sp electrons (Spisák and Hafner, 2002). The induced magnetic moment in the substrate surface, and thus the substrate contribution to the overlayer magnetism, is 1 order of magnitude larger for Pt substrates than for Cu substrates (Ederer, Komelj and Fähnle, 2003; Lazarovits, Szunyogh and Weinberger, 2003). Details of the film-substrate interaction will be discussed in the next section.

Further investigation of the magnetism of Fe/Pt(997) in the thickness range between 0.5 and 5 atomic layers identifies the evolution of the anisotropy for this system during the transition toward 2D layers (Figure 9). The system shows a perpendicular easy magnetization axis up to a film thickness of 3 ML. The reorientation of **M** into the film plane occurs gradually between 2.6 and 3 ML via a canted magnetization state. The spin reorientation is accompanied by a structural transition from fcc(111) to bcc(110) layers with Kurdjumov–Sachs orientation to the substrate. Above 3 ML coverage the easy axis is found within the plane in the direction along the substrate steps. Perpendicular to the steps only hard axis loops with no remanence are found. The strong in-plane anisotropy is attributed to peculiarities of the bcc structure of the film in this thickness range (Repetto

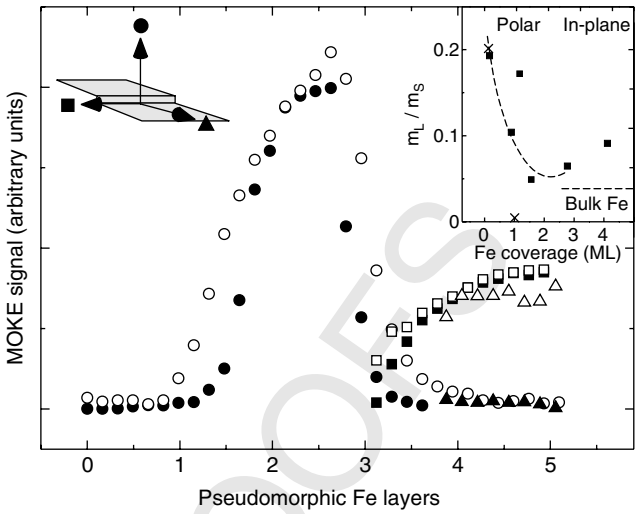

Figure 9. Evolution of the easy magnetization axis for 2D Fe films on Pt substrates with Fe coverage. Open and solid symbols correspond to the saturation and remanent magnetization as obtained from MOKE hysteresis loops at 300 K. A spin reorientation from perpendicular to in-plane direction is observed at the critical thickness of $t_{crit} = 2.8$ atomic layers. Above t_{crit} the films show pronounced in-plane anisotropy with the easy axis along the step edges. Inset: For films thinner than 1 atomic layer the ratio m_L/m_S (from XMCD measurements) increases in favor of larger m_L values, in qualitative agreement with calculations (×, from reference Ederer, Komelj and Fähnle, 2003).

et al., unpublished). It is interesting to note that Fe films on Pt(100) substrate, in contrast, do not show perpendicular magnetization at any thickness (He *et al.*, 2005). The occurrence of perpendicular magnetization in the monolayer thickness range is commonly ascribed to anisotropy contributions arising at the film's interfaces (see recent overview articles on this field, such as Gradmann, 1993; Shen and Kirschner, 2002; Sander, 2004). More detailed analysis connects the perpendicular magnetic anisotropy of this system with the strong film–substrate interaction. The bonding to the substrate in surface normal direction – which is particularly large for Pt substrates – disturbs orbital motion of the electrons perpendicular to the film plane and significantly increases the bandwidth in this direction, thus promoting perpendicular magnetization (Wang, Wu and Freeman, 1994; Stöhr, 1999). The choice of substrate material and the local atomic arrangement within the nanostructures has decisive influence on the magnetic anisotropy, a fact that will be illustrated more profoundly in the following section.

The measurement of the ratio of orbital to spin magnetic moment reveals an enhancement of the ratio $m_L : m_S$ by a factor of 5 when going from bulk to monatomic chains (see inset in Figure 9). This increase is completely attributed to m_L since below 1 ML Fe coverage m_S is expected to change only slightly (Ederer, Komelj and Fähnle, 2003). In

analogy to the discussion of Co clusters in the previous chapter the large m_L is explained by the unquenching of orbital electron motion due to decreased coordination. The latter results in more localized d-bands, and therefore in an increased density of states at E_F and in enhanced moments of the d-electrons. In addition, the exchange splitting between majority and minority electrons is large not only for d-bands but also for sp-bands (Spisák and Hafner, 2002), which may result in sizeable additional contributions to the overall magnetic moment. The minimum in $m_L : m_S$ observed for 1 ML Fe is in qualitative agreement with first principles calculations for Pt-supported fcc(111) Fe monolayers which predict a minimal m_L at this coverage (Ederer, Komelj and Fähnle, 2003).

4.2 High coercivity FePt surface alloy

In Section 3, we elaborated on the importance of high magnetocrystalline anisotropy energy for establishing ferromagnetism in low-dimensional systems. Indeed, nanostructured materials with MCA beyond 10^8 erg cm^{-3} (>1 meV per atom) are being considered for upcoming high-density storage media. Thin films (Yan, Zeng Powers and Sellmyer, 2002; Kanazawa, Lauhoff and Suzuki, 2000; Okamoto *et al*., 2002), multilayers (Johnson, Bloemen, den Broeder and de Vries, 1996), and nanoparticles (Sun *et al*., 2000; Okamoto *et al*., 2002) of intermetallic phases exhibiting the $L1_0$ structure, such as the FePt alloy, fulfill this requirement and are currently in the focus of experimental and theoretical research (2005). The $L1_0$ structure is obtained by alternative stacking of fcc(100) oriented layers of two different materials, such as 3d and 5d elements. Currently, the high anisotropy of FePt alloy is described as the result of 3D coordination of Fe atoms with Pt neighbors. The exchange interaction between Fe atoms across adjacent fcc(100) layers, and hence the 3D nature of the alloy, is considered to be important for large MCA. A key role is played by the induced magnetism in Pt which gives additional MCA contributions due to its large spin-orbit interaction (Ravindran *et al*., 2001). Tetragonal lattice distortion and chemical disorder are found to give access not only to the magnetic anisotropy energy but also to the Curie temperature T_C, exchange interaction J, or saturation magnetization M_S. In this section, we demonstrate on the example of 2D $Fe_{50}Pt_{50}$ surface alloys that the $L1_0$ structure is not required to obtain a large anisotropy. The coordination of Fe with Pt atoms in monolayer thin films increases the MCA so that values close to bulk FePt could be measured (Honolka *et al*., unpublished).

$Fe_{50}Pt_{50}$ surface alloys are obtained by deposition of 0.5 atomic layers of Fe on the Pt(997) substrate at 525 K. The thermally activated diffusion of Fe into the Pt terraces results in the formation of monatomic chain segments of Fe embedded in the Pt surface (Lee, Sarbach, Kuhnke and Kern, unpublished), similar to surface alloying of Fe on Pt(111) (Schmid and Varga, 2002). The average spacing between Fe chain segments depends on the amount of deposited Fe and is 5.54 Å (two Pt row spacings) for the idealized $Fe_{50}Pt_{50}$ surface alloy. The element specificity of the XMCD is ideal for probing the magnetism of the Fe and Pt sublattices separately. Typical XAS and XMCD spectra at the Fe $L_{3,2}$ and the Pt $N_{7,6}$ absorption edges are displayed for $Fe_{50}Pt_{50}$ in Figure 10(a). A large dichroic signal was detected at both absorption edges. The presence of a dichroic signal for Pt is the result of an induced magnetic moment due to the hybridization between Fe 3d and Pt 5d states. The existence of a magnetic moment in Pt evidences ferromagnetic coupling between the Fe chains. Antiferromagnetic ordering of the Fe moments would rather result only in negligible Pt moments (Skomski, Kashyap and Sellmyer, 2003; Skomski, Kashyap and Zhou, 2005). The sign relationship of the XMCD signals at the Fe $L_{3,2}$

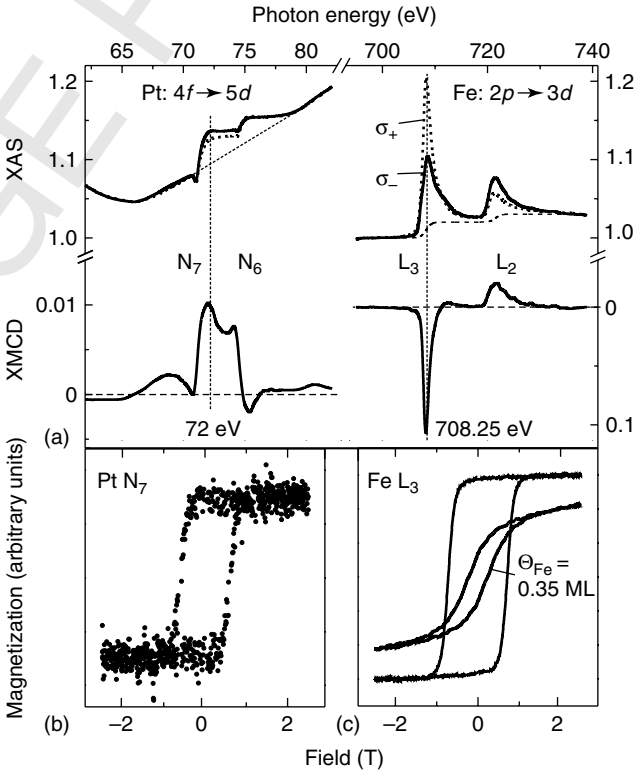

Figure 10. (a) X-ray absorption and XMCD spectra at the Pt $N_{7,6}$ and the Fe $L_{3,2}$ absorption edges of a single, two-dimensional $Fe_{50}Pt_{50}$ surface alloy layer. (b) and (c) The dichroic signal was used to obtain element-specific hysteresis loops of the Fe and Pt sublattice of the same film at 12 ± 1 K. The hysteresis loop of the Fe sublattice is compared to the Fe L_3 loop of a diluted $Fe_{35}Pt_{65}$ monolayer.

and the Pt $N_{7,6}$ absorption edges reveals parallel spin alignment of the Fe and Pt sublattices (Shishidou *et al*., 1997). The coupled magnetization of Fe and Pt results in congruent *M-H* magnetization loops which are obtained at each constituent's absorption edge (Figure 10b and c). The preferential magnetization axis is along the surface normal. The large coercive field of $H_C = 0.71$ T is of the same order of magnitude as the values found for the bulk FePt $L1_0$ phase and demonstrates the presence of a considerable anisotropy energy barrier which should be overcome in order to reverse the magnetization.

From the XMCD spectrum in Figure 10(a) a total spin moment of $(2.4 \pm 0.2)\mu_B$ per Fe atom is determined. This experimental value is 18% smaller than theoretically predicted Fe moments of 2.93 μ_B (Staunton *et al*., 2004a) and 2.92 μ_B (Kashyap *et al*., 2004). The determination of the Pt moment from the N-edge dichroism provides a challenge to theorists since the interaction between discrete-like and continuum states during the $4f \rightarrow 5d$ dipole transition leads to a Fano-type interference effect and have to be treated accordingly (Shishidou *et al*., 1997). As a lower limit, a Pt moment of >0.2 μ_B per Pt atom is estimated from a comparison of the normalized XMCD signals with $CoPt_3$ bulk samples where the Pt moment is known (Menzinger and Paoletti, 1966). This value is close to calculated Pt spin moments of 0.24 μ_B per atom in the top layer of Pt(111) covered by one monolayer of Fe (Ederer, Komelj and Fähnle, 2003), and of 0.29 μ_B (Staunton *et al*., 2004a) and 0.35 μ_B (Kashyap *et al*., 2004) in $L1_0$ ordered FePt. However, at Co/Pt interfaces an induced spin moment as large as 0.53 μ_B per Pt atom has been determined from XMCD measurements at the Pt $L_{2,3}$ edge (Suzuki *et al*., 2005).

The MCA of the surface alloy is calculated from angular dependent XMCD measurements to $K = 0.42$ meV per formula unit. Strikingly, this value for the alloyed monolayer is only about a factor of 2–3 smaller than 0.6–1 meV per atom which is typically found for FePt-$L1_0$ bulk samples (Shima, Moriguchi, Mitani and Takanash, 2002; Shima, Takanashi, Takahashi and Hono, 2002; Farrow *et al*., 1996). As was mentioned already in the preceding text, the MCA is usually related to the orbital moment anisotropy, Δm_L (Bruno, 1989). For the $Fe_{50}Pt_{50}$ surface alloy we determined $\Delta m_L^{alloy} = m_L^{\perp} - m_L^{||} = 0.025 \pm 0.004$ μ_B per hole. This value is close to the measured orbital anisotropy of nonalloyed Fe adlayers on Pt(997) of similar Fe content, $\Delta m_L^{stripe} = 0.035 \pm 0.009$ μ_B per hole. This experimental observation has important implications for the interpretation of the origin of the MCA in alloys, as will be shown in the following text. It is worth to note that both experimental values are by a factor of 2 larger than calculated values, as for instance, in Solovyev, Dederichs and Mertig (1995).

The comparison of the hysteresis loop of $Fe_{50}Pt_{50}$ with those of nonalloyed submonolayer Fe stripes in Figure 8 shows that the alloy has a much stronger tendency toward magnetic ordering, together with a significantly enhanced coercivity. A key role for the conservation of the saturation magnetization in remanence observed for the 2D alloy, and more importantly for the large anisotropy, is obviously played by the magnetism of the Pt atoms. Although the induced exchange splitting in Pt is much weaker than in bulk Fe, its spin-orbit coupling is 1 order of magnitude larger ($\xi_{Pt} = 0.6$ eV Misemer, 1988 vs $\xi_{Fe} = 0.07$ eV Mackintosh and Andersen, 1980). In result, the Pt orbital moments are expected to be comparable to those of Fe (comparable also to induced Pt orbital moments in the vicinity of Fe chains, $m_L \approx 0.04$ μ_B Ederer *et al*., 2003). In this simple but quite instructive picture the Fe acts only as the source of magnetization, whereas the Pt sublattice, owing to its large spin-orbit interaction, provides the main contribution to the large MCA. Attempts have been made to express the MCA of binary and multicomponent systems by the sum of the magnetic anisotropy of each constituent (Ravindran *et al*., 2001; Solovyev, Dederichs and Mertig, 1995). This means that the total MCA is made large by the spin-orbit coupling of the Pt, while the orbital anisotropy of Fe alone remains unchanged – something that our experimental values in the preceding text show. Support of this viewpoint comes from calculations, showing that suppressing the spin-orbit interaction in the 4d/5d constituent reduces the calculated total anisotropy (Burkert *et al*., 2005; Daalderop, Kelly and Schuurmans, 1990).

As has been discussed by several authors, the description of MCA is complicated by chemical disorder (Brown *et al*., 2003; Skomski, Kashyap, Zhou 2005; Okamoto *et al*., 2002; Staunton *et al*., 2004b; Sun *et al*., 2000; Burkert *et al*., 2005), tetragonal distortion (Ravindran *et al*., 2001; Brown *et al*., 2003; Burkert *et al*., 2005), dimensionality, local atomic coordination, and crystal field asymmetry (Ravindran *et al*., 2001). For the surface alloys in this section the chemical disorder, that is, 3d and 5d substitutions as schematically shown in Figure 11(b), plays an important role. Fe atoms in antisite positions bridge the Pt chains and are found to stabilize ferromagnetic ordering of the Fe sublattice, which is predicted to be antiferromagnetic in the ideal structure as in Figure 11(a) (Brown *et al*., 2003). Such disorder can also be assumed to reduce the in-plane magnetic anisotropy of the alloy drastically, as was found experimentally (Honolka *et al*., unpublished).

The experiments point out that the coordination of Fe atoms with Pt, along with strong covalent 3d–5d hybridization, is necessary to achieve large MCA. The importance of Fe-Pt coordination is demonstrated by comparing the hysteresis loop of the $Fe_{50}Pt_{50}$ surface alloy with that of a Fe-poor,

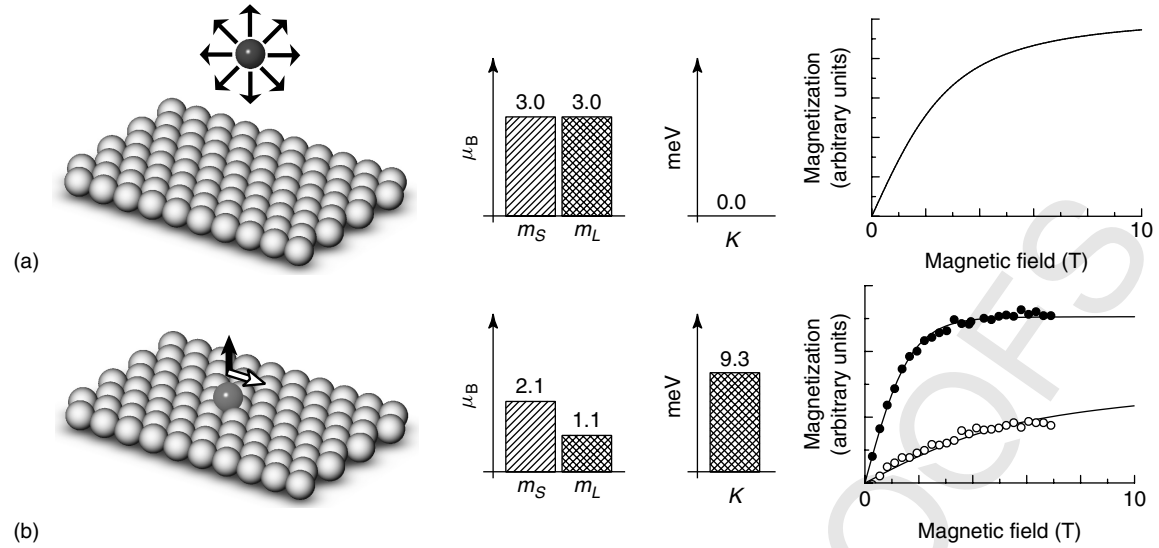

Figure 11. Ordered (a) and disordered (b) structure of a linear, two-dimensional FePt surface alloy. Fe and Pt atoms are represented by dark and bright colors. Deviations from the ideal structure result mostly in ferromagnetic interchain bridges, which promote ferromagnetism in the Fe sublattice and reduce the in-plane anisotropy.

diluted $Fe_{35}Pt_{75}$ surface alloy (Figure 10c). Reducing of the Fe concentration by only 30% results in S-shaped loops with the remanence reduced by 78% and the coercivity by 68%. The shape of the loop is similar to the magnetization curve of the nonalloyed Fe stripe in Figure 8(c), for which full spin alignment has only been achieved in external fields of $H > 6$ T. One can say that the increased average spacing between Fe atoms destabilizes the magnetization. It leads on the one hand to narrower Fe d-bands, and in consequence to reduced hybridization and smaller anisotropy. On the other hand, separation of Fe chains by more than one Pt covalent radius significantly decreases the induced net moment in Pt (Ederer, Komelj and Fähnle, 2003) and hence diminishes the Pt's contribution to the magnetism of the surface layer. This is consistent with the observation that Fe-poor FePt bulk alloys exhibit reduced stability of the ferromagnetic order (Brown *et al*., 2003).

5 CONCLUSION

With the ability to control the fabrication of 0D, 1D, and 2D structures of 3d metals by self-organized growth we are capable to study magnetic phenomena in solid-state systems with atomic scale control over their size and crystalline structure. Co and Fe structures of reduced dimensionality reveal a strikingly rich magnetic behavior. Impurity atoms of Co on Pt surfaces have extraordinarily large MCA values and spin and orbital moments halfway between the values of free atoms and bulk Co. The MCA is decreasing with increasing Co coordination when forming small clusters or chains, but still sufficiently large in monatomic Co chains to stabilize a ferromagnetic long-range ordered state at finite temperature. The effect of local atomic coordination on the magnetism of Co and Fe manifests itself in the observed fluctuations of the easy axis with increasing stripe width, as well as in strong orbital magnetism. In all structures investigated a key role is played by the supporting substrate. Pt is found to contribute to the nanostructure's MCA via strong electronic hybridization and even dominates the magnetic anisotropy in the FePt surface alloy. An important consequence of the hybridization is the induced magnetization in Pt.

The basic experiments presented in this chapter contribute to a fundamental understanding of the magnetic properties of finite-sized particles. These results further elucidate the interplay between local coordination, orbital magnetism, and magnetic anisotropy. The link is provided by the electronic structure of the d-states, which sensitively responds to the local atomic arrangement, that is, the number and the electronic nature of the neighboring atoms as well as their interatomic spacing. This knowledge is not only of importance for testing detailed theoretical models used in the prediction and interpretation of magnetic phenomena but also for the conceptual design of nanosized magnetic structures that elude the superparamagnetic limit. In this context, our data show that particles containing only about 400 Co atoms can behave as ferromagnets at room temperature. Besides the geometry of the atomic arrangement, additional leverage on the magnetic properties is obtained from the choice of the material of the coordinating atoms. When forming a binary alloy the overall magnetism strongly depends also on the nonmagnetic constituent. This is particularly true for

nanostructures, such as for the FePt surface alloy, where the low-coordinated Pt atoms acquire a sizeable magnetic moment and contribute with their large spin-orbit coupling to the total magnetic anisotropy.

The work presented in this chapter has only just opened the door toward complex and functional nanostructure networks. Expanded and highly ordered 2D and even 3D networks of nanoscale building blocks can be fabricated by self-organized growth, aided by functionalized molecules, biotemplates or in combination with top-down approaches. It is expected that magnetic nanostructures will play a key role to add functionality to such structures by exploiting their magnetic moments and magnetic ordering associated with magneto-transport or quantum effects. Future experiments may show and exploit ferromagnetism in nanostructures of elements which are non-magnetic in the bulk, thus opening up additional possibilities. At the frontiers to atomic and nanometer scale structures we will enjoy virtually unlimited avenues for research and promising chances for applications in the near future.

ACKNOWLEDGMENTS

The authors would like to thank Jan Honolka, Klaus Kuhnke, Kai Fauth, Arne Dallmeyer, Carlo Carbone, Stefano Rusponi, Harald Brune, and Sarnjeet S. Dhesi for their valuable contributions to this work.

REFERENCES

Q9
Q10

Apsel, S.E., Emmert, J.W., Deng, J. and Bloomfield, L.A. (1996). *Physical Review Letters*•, **76**, 1441.

Bansmann, J., Baker, S., Binns C., *et al*. (2005). • *Surface Science Reports*, **56**, 189.

Barth, J.V., Brune, H., Ertl, G. and Behm, R.J. (1990). *Physical Review B*, **42**, 9307–9318.

Bellini, V., Papanikolaou, N., Zeller, R. and Dederichs, P.H. (2001). *Physical Review B*, **64**, 094403.

Billas, I.M.L., Chatelain, A. and de Heer, W.A. (1994). *Science*, **265**, 1682.

Bland, J.A.C. and Heinrich, B. (Eds.) (2005). *Ultrathin Magnetic Structures I*, Springer: Berlin.

Blügel, S. (2007). *Handbook of Magnetism and Advanced Magnetic Materials*, John Wiley & Sons: Chichester.

Boeglin, C., Stanescu, J.P., Deville, P., *et al*. (2002). *Physical Review B*, **66**, 014439.

Bogani, L., Caneschi, A., Fedi M., *et al*. (2004). *Physical Review Letters*, **92**, 207204.

Bonnenberg, D., Hempel, K.A. and Wijn, H.P.J. (1986). In *Magnetic Properties of 3d, 4d, and 5d Elements, Alloys and Compounds*, *Landolt-Bornstein, New Series*, Hellwege, K.-H. and Madelung, O. (Eds.), Springer-Verlag: Berlin, p. 178, Vol. III/19a.

Brown, G., Kraczek, B., Janotti A., *et al*. (2003). *Physical Review B*, **68**, 052405.

Brune, H., Giovannini, M., Bromann, K. and Kern, K. (1998). *Nature*, **394**, 451–453.

Brune, H., Roder, H., Boragno, C. and Kern, K. (1994). *Physical Review B*, **49**, 2997–3000.

Brune, H., Romainczyk, C., Roder, H. and Kern, K. (1994). *Nature*, **369**, 469–471.

Brune, H., Roder, H., Bromann, K., *et al*. (1996). *Surface Science*, **349**, L115–L122.

Bruno, P. (1989). *Physical Review B*, **39**, 865.

Bruno, P. (2001). *Physical Review Letters*, **87**, 137203.

Bruno, P. and Sandratskii, L.M. (2005). *Physical Journal*, **4**(5), 21.

Burkert, T., Eriksson, O., Simak S.I., *et al*. (2005). *Physical Review B*, **71**, 134441.

Caneschi, A., Gatteschi, D., Lalioti N., *et al*. (2001). *Angewandte Chemie (International ed. in English)*, **40**, 1760.

Carra, P., Thole, B.T., Altarelli, M. and Wang, X. (1993). *Physical Review Letters*, **70**, 694.

Chambliss, D.D., Wilson, R.J. and Chiang, S. (1991). *Physical Review Letters*, **66**, 1721–1724.

Chen, C.T., Idzerda, Y.U., Lin H.-J., *et al*. (1995). *Physical Review Letters*, **75**, 152.

Clemens, W., Kachel, T., Rader O., *et al*. (1992). *Solid State Communications*, **81**, 739.

Clérac, R., Miyasaka, H., Yamashita, M. and Coulon, C. (2002). *Journal of the American Chemical Society*, **124**, 12837.

Daalderop, G.H.O., Kelly, P.J. and Schuurmans, M.F.H. (1990). *Physical Review B*, **42**(11), 7270.

Dallmeyer, A., Carbone, C. Eberhardt, W., *et al*. (2000). *Physical Review B*, **61**, R5133.

De Jongh, L.J. and Miedema, A.R. (1974). *Advances in Physics*, **23**, 1.

Dingle, R., Lines, M.E. and Holt, S.L. (1969). *Physical Review*, **187**, 643.

Dorantes-Dávila, J. and Pastor, G.M. (1998). *Physical Review Letters*, **81**(1), 208.

Dupas, C., Renard, J.P., Seiden, J. and Cheikh-Rouhou, A. (1982). *Physical Review B*, **25**, 3261.

Dürr, H.A., Dhesi, S.S., Dudzik E., *et al*. (1999). *Physical Review B*, **59**, R701.

Dürr, H.A., Guo, G.Y., van der Laan G., *et al*. (1997). *Science*, **277**, 213.

Ederer, C., Komelj, M. and Fähnle, M. (2003). *Physical Review B*, **68**, 52402.

Edmonds, K.W., Binns, C., Baker, S.H., *et al*. (1999). *Physical Review B*, **60**(1), 472.

Ehrlich, G. and Hudda, F.G. (1966). *Journal of Chemical Physics*, **44**, 1039.

Elmers, H.J., Hauschild, J., Höche, H., *et al*. (1994). *Physical Review Letters*, **73**(6), 898.

Farrow, R.F.C., Weller, D., Marks, R.F., *et al*. (1996). *Journal of Applied Physics*, **79**(8), 5967.

Félix-Medina, R., Dorantes-Dávila, J. and Pastor, G.M. (2002). *New Journal of Physics*, **4**, 100.

Fischer, B., Brune, H., Barth, J. V., *et al*. (1999). *Physical Review Letters*, **82**, 1732–1735.

Frôta-Pessoa, S., Muniz, R.B. and Kudrnovský, J. (2000). *Physical Review B*, **62**, 5293.

Fruchart, O., Eleoui, M., Vogel, J., *et al*. (2004). *Applied Physics Letters*, **84**(8), 1335.

Fruchart, O., Klaua, M., Barthel, J. and Kirschner, J. (1999). *Physical Review Letters*, **83**, 2769–2772.

Gambardella, P., Blanc, M., Brune H., *et al*. (2000). *Physical Review B*, **61**, 2254.

Gambardella, P., Dallmeyer, A., Maiti K., *et al*. (2002a). *Nature*, **416**, 301.

Gambardella, P., Dhesi S.S., Gardonio S., *et al*. (2002b). *Physical Review Letters*, **88**, 047202.

Gambardella, P., Dallmeyer, A., Maiti K., *et al*. (2004). *Physical Review Letters*, **93**, 077203.

Gambardella, P., Rusponi, S., Veronese M., *et al*. (2003). *Science*, **300**, 1130.

Glauber, R.J. (1963). *Journal of Mathematical Physics*, **4**, 294.

Gradmann, U. (1993). In *Handbook of Magnetic Materials*, Buschow, K.H.J. (Ed.), Elsevier Science Publishers B. V.: New York, Vol. 7.

Hahn, E., Schief, H., Marsico, V., *et al*. (1994). *Physical Review Letters*, **72**, 3378–3381.

Hauschild, J., Elmers, H.J. and Gradmann, U. (1998). *Physical Review B*, **57**, R677.

He, K., Zhang, L.J., Ma, X.C., *et al*. (2005). *Physical Review B*, **72**, 155432.

Himpsel, F.J., Ortega, J.E., Mankey, G.J. and Willis, R.F. (1998). *Advances in Physics*, **47**, 511.

Hone, D.W. and Richards, P.M. (1974). *Annual Review of Materials Science*, **4**, 337.

Hong, J. and Wu, R.Q. (2003). *Physical Review B*, **67**, 020406.

Hong, J. and Wu, R.Q. (2004). *Physical Review B*, **70**, 060406.

Honolka, J., *et al*. unpublished●.

Hwang, R.Q., Schroder, J., Gunther, C. and Behm, R.J. (1991). *Physical Review Letters*, **67**, 3279–3282.

Ising, E. (1925). *Zeitschrift Fur Physik*, **31**, 253.

Jansen, R. and Moodera, J.S. (1998). *Journal of Applied Physics*, **83**, 6682.

Jin, Y.J., Kim, I.G. and Lee, J.I. (2004). *Physica Status Solidi B-Basic Research*, **241**(7), 1431.

Johnson, M.T., Bloemen, P.J.H., den Broeder, F.J.A. and de Vries, J.J. (1996). *Reports on Progress in Physics*, **59**, 1409.

Kanazawa, H., Lauhoff, G. and Suzuki, T. (2000). *Journal of Applied Physics*, **87**, 6143.

Kashyap, A., Skomski, R., Solanki, A.K., *et al*. (2004). *Journal of Applied Physics*, **95**(11), 7480.

Kawagoe, T., Sogabe, K., Kondoh, N., *et al*. (1998). *Japanese Journal of Applied Physics*, **37**, 3796.

Kirakosian, A., Bennewitz, R., Crain J.N., *et al*. (2001). *Applied Physics Letters*, **79**, 1608–1610.

Klein, A., Schmidt, A., Hammer, L. and Heinz, K. (2004). *Europhysics Letters*, **65**(6), 830.

Knickelbein, M.B. (2001). *Physical Review Letters*, **86**, 5255.

Koide, T., Miyauchi, H., Okamoto, J., *et al*. (2001). *Physical Review Letters*, **87**, 257201.

Komelj, M., Ederer, C., Davenport, J.W. and Fähnle, M. (2002). *Physical Review B*, **66**, 140407.

Kronmüller, H. (2003). *Micromagnetism and The Microstructure of Ferromagnetic Solids*, Cambridge University Press: Cambridge.

van der Laan, G. and Thole, B.T. (1991). *Physical Review B*, **43**, 13401.

Landau, L.D. and Lifshitz, E.M. (1959). In *Statistical Physics*, Pergamon: London, p. 482, Vol. 5.

Landee, C.P. and Willett, R.D. (1979). *Physical Review Letters*, **43**, 463.

Lau, J.T., Föhlisch, A., Nietubyc, R., *et al*. (2002). *Physical Review Letters*, **89**, 057201.

Lazarovits, B., Szunyogh, L. and Weinberger, P. (2003). *Physical Review B*, **67**, 024415.

Lazarovits, B., Szunyogh, L., Weinberger, P. and Újfalussy, B. (2003). *Physical Review B*, **68**, 024433.

Lee, T.Y., Sarbach, S., Kuhnke, K. and Kern, K. ●unpublished. CondMat 0504337.

Leroy, F., Eymery, J., Gentile, P. and Fournel, F. (2002). *Applied Physics Letters*, **80**, 3078–3080.

Lescouëzec, R., Vaissermann, J., Ruiz-Pérez, C., *et al*. (2003). *Angewandte Chemie (International ed. in English)*, **42**, 1483.

Li, D., Cuenya, B.R., Pearson, J., *et al*. (2001). *Physical Review B*, **64**, 144410.

Li, Y.G., *et al*. (1997). *Physical Review B*●, **56**, 12539–12543.

Lin, J.L., Petrovykh, D.Y., Kirakosian, A., *et al*. (2001). *Applied Physics Letters*, **78**, 829.

Ma, X., Meyerheim, H.L., Barthel, J., *et al*. (2004). *Applied Physics Letters*, **84**(20), 4038.

Mackintosh, A.R. and Andersen, O.K. (1980). In *Electrons at the Fermi Surface*, Springford, M. (Eds.), Cambridge University Press: Cambridge, p. 149.

Martins, M., Godehusen, K., Richter, T. and Zimmermann, P. (2003). *Aip Conference Proceedings*, **652**, 153.

Menzinger, F. and Paoletti, A. (1966). *Physical Review*, **143**, 365.

Mermin, N.D. and Wagner, H. (1966). *Physical Review Letters*, **17**, 1133.

Michely, T. and Comsa, G. (1991). *Surface Science*, **256**, 217–226.

Misemer, D.K. (1988). *Journal of Magnetism and Magnetic Materials*, **72**, 267.

Mo, Y.W., Kleiner, J., Webb, M.B. and Lagally, M.G. (1991). *Physical Review Letters*, **66**, 1998–2001.

Morgenstern, K., Rosenfeld, G. and Comsa, G. (1996). *Physical Review Letters*, **76**, 2113–2116.

Q11

Q12

Q13

Mydosh, J.A. and Nieuwenhuys, G.J. (1980). In *Ferromagnetic Materials*, Wohlfarth, E.P. (Ed.), North-Holland: Amsterdam, p. 7.

Nakajima, N., Koide, T., Shidara, T., *et al*. (1998). *Physical Review Letters*, **81**, 5229.

Nonas, B., Cabria, I., Zeller, R., *et al*. (2001). *Physical Review Letters*, **86**, 2146.

Nötzel, R. (1996). *Semiconductor Science and Technology*, **11**, 1365–1379.

Ohresser, P., Brookes, N.B., Padovani, S., *et al*. (2001). *Physical Review B*, **64**, 104429.

Okamoto, S., Kikuchi, N., Kitakami, O., *et al*. (2002). *Physical Review B*, **66**, 024413.

Okamoto, S., Kitakami, O., Kikuchi, N., *et al*. (2002). *Physical Review B*, **66**, 24413.

Q14 Overview on $L1_0$ magnetism in (2005). *Scripta Materialia*, **53** 381, and following• articles.

Pajda, M., Kudrnovský, J., Turek, I., *et al*. (2000). *Physical Review Letters*, **85**(25), 5424.

Pajda, M., Kudrnovský, J., Turek, I., *et al*. (2001). *Physical Review B*, **64**, 174402.

Pimpinelli, A., Villain, J. and Wolf, D.E. (1992). *Physical Review Letters*, **69**, 985–985.

Poulopoulos, P. and Baberschke, K. (1999). *Journal of Physics-Condensed Matter*, **11**, 9495.

Pratzer, M., Elmers, H.J., Bode, M., *et al*. (2001). *Physical Review Letters*, **87**, 127201.

Ravindran, P., Kjekshus, A., Fjellvåg, H., *et al*. (2001). *Physical Review B*, **63**, 144409.

Q15 Repetto, D., Lee, T.Y., Honolka, J., *et al*. •unpublished.

Röder, H., Hahn, E., Brune, H., *et al*. (1993). *Nature*, **366**, 141–143.

Rodrigues, V., Bettini, J., Silva, P.C. and Ugarte, D. (2003). *Physical Review Letters*, **91**, 096801.

Rusponi, S., Cren, T., Weiss, N., *et al*. (2004). *Nature Materials*, **2**, 546.

Sander, D. (2004). *Journal of Physics-Condensed Matter*, **16**, R603–R636.

Schmid, M. and Varga, P. (2002). *Chemistry and Physics of Solid Surface*, **10**, 118–151.

Schneider, C.M. and Kirschner, J. (2000). In *Handbook of Surface Science*, Horn, K. and Scheffler, M. (Eds.), Elsevier: Amsterdam, p. 511, Vol. 2.

Schneider, C.M., de Miguel, J.J., Bressler, P., *et al*. (1990). *Journal of Electron Spectroscopy and Related Phenomena*, **51**, 263.

Shen, J. and Kirschner, J. (2002). *Surface Science*, **500**, 300.

Shen, J., Klaua, M., Ohresser, P., *et al*. (1997a). *Physical Review B*, **56**, 11134.

Shen, J., Skomski, R., Klaua, M., *et al*. (1997b). *Physical Review B*, **56**, 2340.

Shick, A.B., Máca, F. and Oppeneer, P.M. (2004). *Physical Review B*, **69**, 212410.

Shick, A.B., Máca, F. and Oppeneer, P.M. (2005). *Journal of Magnetism and Magnetic Materials*, **290–291**, 257.

Shima, T., Moriguchi, T., Mitani, S. and Takanashi, K. (2002). *Applied Physics Letters*, **80**(2), 288.

Shima, T., Takanashi, K., Takahashi, Y.K. and Hono, K. (2002). *Applied Physics Letters*, **81**(6), 1050.

Shiraki, S., Fujisawa, H., Nantoh, M. and Kawai, M. (2004). *Applied Surface Science*, **237**, 284.

Shiraki, S., Fujisawa, H., Nantoh, M. and Kawai, M. (2005). *Journal of the Physical Society of Japan*, **74**(7), 2033.

Q16 Shishidou, T., Imada, S., Muro, T., *et al*. (1997). •*Physical Review B*, **55**, 3749.

Skomski, R. and Coey, J.M.D. (1999). *Permanent Magnetism*, Institute of Physics Publishing: Bristol.

Skomski, R., Kashyap, A. and Sellmyer, D.J. (2003). *IEEE Transactions on Magnetics*, **39**, 2917.

Skomski, R., Kashyap, A. and Zhou, J. (2005). *Scripta Materialia*, **53**, 389.

Solovyev, I.V., Dederichs, P.H. and Mertig, I. (1995). *Physical Review B*, **52**(18), 13419.

Song, F. and Bergmann, G. (2001). *Physical Review Letters*, **86**, 2138.

Spisák, D. and Hafner, J. (2002). *Physical Review B*, **65**, 235405.

Spisák, D. and Hafner, J. (2003). *Physical Review B*, **67**, 214416.

Staunton, J.B., Ostantin, S., Razee, S.S.A., *et al*. (2004a). *Physical Review Letters*, **93**, 257204.

Staunton, J.B., Ostantin, S., Razee, S.S.A., *et al*., (2004b). *Journal of Physics-Condensed Matter*, **16**, S5623.

Stepanyuk, V.S., Hergert, W., Wildberger, K., *et al*. (1996). *Physical Review B*, **53**(4), 2121.

Stöhr, J. (1999). *Journal of Magnetism and Magnetic Materials*, **200**, 470.

Stumpf, R. and Scheffler, M. (1994). *Physical Review Letters*, **72**, 254–257.

Sun, S., Murray, C.B., Weller, D., *et al*. (2000). *Science*, **287**, 1989.

Suzuki, M., Muraoka, H., Inaba, Y., *et al*. (2005). *Physical Review B*, **72**, 054430.

Temmyo, J., Kuramochi, E., Kamada, H. and Tamamura, T. (1998). *Journal of Crystal Growth*, **195**, 516–523.

Thole, B.T., Carra, P., Sette, F. and Van der Laan, G. (1992). *Physical Review Letters*, **68**, 1943.

Tischer, M., Hjortstam, O., Arvanitis, D., *et al*. (1995). *Physical Review Letters*, **75**, 1602.

Újfalussy, B., Lazarovits, B., Szunyogh, L., *et al*. (2004). *Physical Review B*, **70**, 100404.

Vindigni, A., Rettori, A., Pini, M.G., *et al*. (2006). *Applied Physics A*, **82**, 385–394.

Wang, D.S., Wu, R. and Freeman, A.J. (1994). *Journal of Magnetism and Magnetic Materials*, **129**, 237.

Weinert, M. and Freeman, A.J. (1983). *Journal of Magnetism and Magnetic Materials*, **38**, 23.

Weller, D. and Moser, A. (1999). *IEEE Transactions on Magnetics*, **35**, 4423.

Weller, D., Stöhr, J., Nakajiama, R., *et al*. (1995). *Physical Review Letters*, **75**(20), 3752.

Witten, T.A. and Sander, L.M. (1981). *Physical Review Letters*, **47**, 1400–1403.

Wu, R., Li, C. and Freeman, A.J. (1991). *Journal of Magnetism and Magnetic Materials*, **99**, 71.

Yan, L., Przybylski, M., Lu, Y., *et al*. (2005). *Applied Physics Letters*, **86**, 102503.

Yan, M.L., Zeng, H., Powers, N. and Sellmyer, D.J. (2002). *Journal of Applied Physics*, **91**, 8471.

Zhang, Z.Y., Chen, X. and Lagally, M.G. (1994). *Physical Review Letters*, **73**, 1829–1832.

FURTHER READING

Aguilera-Granja, F., Montejano-Carrizales, J.M. and Morán-López, J.L. (1998). *Physics Letters A*, **242**, 255.

Barth, J.V. (2000). *Surface Science Reports*, **40**, 75–150.

Bromann, K., Felix, C., Brune, H., *et al*. (1996). *Science*, **274**, 956.

Brune, H., Roder, H., Boragno, C. and Kern, K. (1994). *Physical Review Letters*, **73**, 1955–1958.

Chikazumi, S. (1997). *Physics of Ferromagnetism*, *Second Edition*, Oxford University Press, p. 546.

Dürr, H.A., van der Laan, G. and Thole, B.T. (1996). *Physical Review Letters*, **76**, 3464.

Garibay-Alonso, R. and López-Sandoval, R. (2005). *Solid State Communications*, **134**, 503.

Guirado-López, R.A., Dorantes-Dávila, J. and Pastor, G.M. (2003). *Physical Review Letters*, **90**(22), 226402.

Haley, C. and Weaver, J. (2002). *Surface Science*, **518**, 243.

Huang, L., Chey, S.J. and Weaver, J. (1998). *Physical Review Letters*, **80**(18), 4095.

Kechrakos, D. and Trohidou, K. (1998). *Physical Review B*, **58**, 12169.

Knorr, N., *et al*., (2002). *Physical Review B*●, **65**.

van der Laan, G. (1998). *Journal of Physics-Condensed Matter*, **30**, 3239.

Lee, H.K., Schulthess, T.C., Landau, D.P., *et al*. (2002). *Journal of Applied Physics*, **91**(10), 6926.

Novosad, V., Guslienko, K.Y., Shima, H., *et al*. (2002). *Physical Review B*, **65**, 60402.

Ohresser, P., Ghiringhelli, G., Tjernberg, O., *et al*. (2000). *Physical Review B*, **62**, 5803.

Pierce, J., Torija, M., Gai, Z., *et al*. (2004). *Physical Review Letters*, **92**(23), 237201.

Repetto, D., Honolka, J., Rusponi, S., *et al*. (2005). *Applied Physics Letters*, ●accepted.

Shen, J., Pierce, J.P., Plummer, E.W. and Kirschner, J. (2003). *Journal of Physics-Condensed Matter*, **15**, R1.

Sipr, O., Košuth, M. and Ebert, H. (2004). *Physical Review B*, **70**, 174423.

Wang, D.S., Wu, R. and Freeman, A.J. (1993). *Physical Review B*, **48**, 15886.

Wang, D.S., Wu, R. and Freeman, A.J. (1994). *Journal of Applied Physics*, **75**(10), 6409.

Weaver, J. and Antonov, V.N. (2004). *Surface Science*, **557**(1–3), 1.

Weaver, J. and Waddill, G. (1991). *Science*, **251**, 1444.

Zhao, J., Chen, X., Sun, Q., *et al*. (1995). *Physics Letters A*, **205**, 308.

An STM movie for Cu diffusion on the Cu(111) surface is shown at http://www.mpi-stuttgart.mpg.de/kern/res_act/supmat_1.html●.

Please note that the abstract and keywords will not be included in the printed book, but are required for the online presentation of this book which will be published on Wiley InterScience (www.interscience.wiley.com). If the abstract and keywords are not present below, please take this opportunity to add them now.

The abstract should be of short paragraph upto 100 words in length and keywords not less than 10 words.

ABSTRACT: The chapter "Magnetism of low-dimensional metallic structures" reviews experiments on the magnetism of surface-supported low-dimensional structures of 3d metals. Controlling the static and dynamic magnetic behavior of both individual impurities and supported nanostructures on nonmagnetic surfaces represents a fundamental challenge as well as a prerequisite to design magnetic storage and logic devices of novel conception. We describe the governing principles of self-organized growth of metallic nanostructures at surfaces and outline approaches to drive and steer self-assembly processes. The controlled assembly of metal nanostructures on crystalline surfaces combined with scanning probe measurements and synchrotron radiation spectroscopy allows us to track the evolution of the magnetic properties from single atoms to finite-sized particles, atomic chains, and two-dimensional layers, highlighting the significance of size, coordination, and interface effects at the atomic scale. As examples, we report on the giant magnetic anisotropy and unquenched orbital moments observed in nanoparticles, unusual oscillations of the easy axis of magnetization in atomic chains of variable thickness, and metastable ferromagnetic order in one-dimension. We discuss the important role played by interactions with a nonmagnetic substrate and point out approaches to control and tune magnetism in nanoscale structures by taking advantage of coordination and hybridization effects.

KEYWORDS: epitaxial growth, self-assembly, magnetism, magnetic anisotropy, atomic chains, clusters, nanoparticles, Fe, Co, FePt alloy, STM, XMCD, MOKE.

QUERIES TO BE ANSWERED BY AUTHOR (SEE MARGINAL MARKS Q..)

IMPORTANT NOTE: You may answer these queries by email. If you prefer, you may print out the PDF, and mark your corrections and answers directly on the proof at the relevant place. Do NOT mark your corrections on this query sheet. Please see the proofing instructions for information about how to return your corrections and query answers.

Q1. Please spell out the initials for all authors.
Q2. There was a mismatch between the figures and their captions. We have matched the figure captions with the appropriate figures. Please confirm if this is correct.
Q3. Please provide the specific chapter numbers that are being referred.
Q4. Please confirm if this abbreviation needs to be spelt out. If yes, please provide the expansion.
Q5. Please confirm if this abbreviation needs to be spelt out. If yes, please provide the expansion.
Q6. Please mention the chapter number.
Q7. Please clarify if this part of the sentence needs to be rephrased. If yes, please provide the rephrased sentence.
Q8. Please clarify if ML denotes monolayer. If yes, please confirm if it should be mentioned within paranthesis.
Q9. Please provide the article title for all the journal references.
Q10. Abbreviated journal titles have been expanded where necessary. Please check that all journal titles are correct in your References and Further Reading list.
Q11. Please clarify if this article has since been published. If so, please provide the complete details for this reference.
Q12. Please clarify if this article has since been published. If so, please provide the complete details for this reference.
Q13. Please list out two more author names for this reference.
Q14. Please provide the complete details for this reference.
Q15. Please clarify if this article has since been published. If so, please provide the complete details for this reference.
Q16. Please confirm if the given information is correct.
Q17. Please provide two more author names and page range for this reference.
Q18. Please clarify if this article has since been published. If so, please provide the volume number and page range for this reference.
Q19. Please provide the access year for this reference.